CHAPTER 4

Results and Discussion (Part I):

Lead Magnesium Niobate and Lead Titanate

In this chapter, the results are presented of the investigation of both powder and ceramic forms of lead magnesium niobate (PMN) and lead titanate (PT), these being the two end components of the PMN-PT system. Phase formation-structure-processing relationships are brought out for each component, and discussed in terms of phase formation, morphology, particle size, densification, crystal structure and microstructure. Attention is first paid to the PMN component, before moving on to the PT component.

4.1 Lead Magnesium Niobate

Before embarking on the fabrication of PMN ceramics, it is appropriate here to focus initially on the preparation of PMN powders. A perovskite-like phase of lead magnesium niobate (PMN) powders has been synthesised by employing the intermediate precursor $MgNb_2O_6$ (MN) in a columbite-like phase. At the first step, the synthesis of single-phase MN powder has been performed with formation of columbite phase investigated as a function of calcination conditions by TG/DTA, XRD and SEM techniques.

4.1.1 Magnesium niobate powders

4.1.1.1 Thermal analysis

The TG and DTA curves recorded at a heating rate of 10 °C/min in air for an equimolar mixture of magnesium oxide and niobium oxide are given in Fig. 4.1. It is seen that TG curve demonstrates two distinct weight loss below 600 °C. The first weight loss occurs below 200 °C and the second one above 250 °C. In the temperature range

from room temperature to ~ 150 °C, the sample shows small exothermic peak in the DTA curve at ~ 120 °C, which is related to the first weight loss. This DTA peak can be attribute to the decomposition of organic species from the milling process.[42] After the first weight loss, the sample shows a steady weight loss over the temperature range of ~ 200-300 °C, followed by a sharp fall in specimen weight with increasing temperature from 250-350 °C.

Corresponding to the second fall in specimen weight (~ 1.8 %), by increasing the temperature up to ~ 700 °C, the solid-state reaction occurs between magnesium oxide and niobium oxide. The broad exothermic characteristic in the DTA curve represents that reaction, which has a maximum at ~ 500 °C. Moreover, another exothermic peaks with maximum at ~ 660 °C was also observed in this profile. These temperatures having been obtained from the calibration of the sample thermocouple. It is to be noted that there is no obvious interpretation of the peaks, although it is likely to correspond to a phase transition reported by a number of researchers.[19,20,23] These data were used to define the ranges of temperatures (500 to 1100 °C) for XRD investigation.

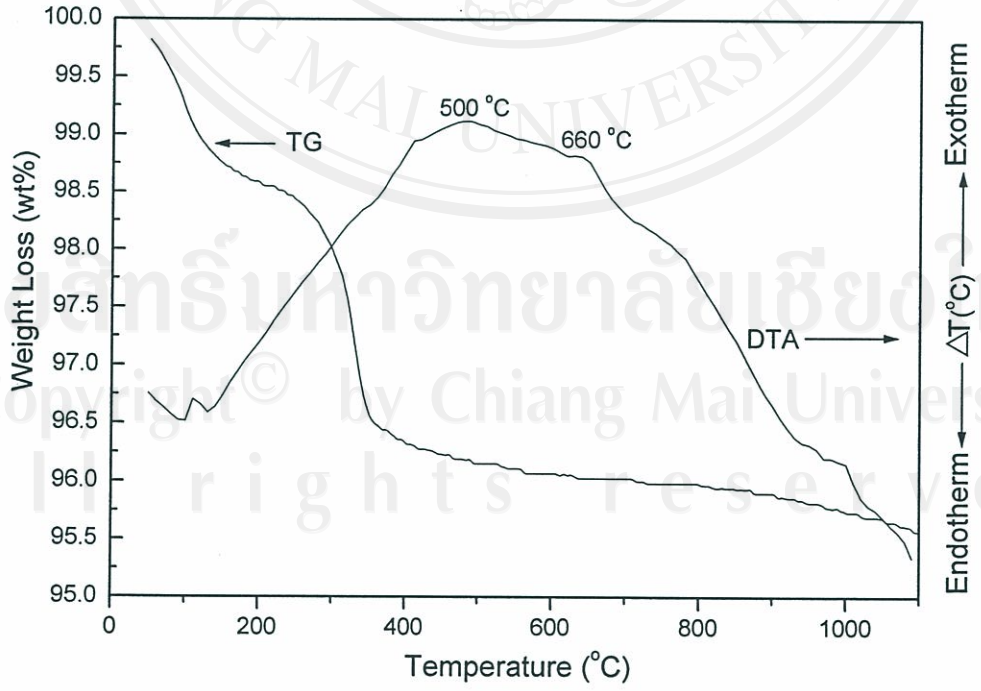

Fig. 4.1 TG and DTA curves for the mixture of MgO-Nb_2O_5 powders.

4.1.1.2 Phase analysis

All calcined powders, together with that of the starting powder mixtures were examined by XRD in order to investigate the phase development (Figs. 4.2-4.4). As shown in Fig. 4.2, unreacted MgO and Nb_2O_5 phases are detected from the original mixture up to 950 °C, whereas minor amount of $MgNb_2O_6$ is observed at 500 °C. By increasing the calcination temperature from 500 to 1100 °C, the yield of $MgNb_2O_6$ phase increases significantly until at 1100 °C, a single phase of $MgNb_2O_6$ is formed, revealing that MgO has completely reacted with Nb_2O_5 phase. This major phase, which could be matched with JCPDS file no. 33-875, possesses an orthorhombic columbite-type structure with lattice parameters a = 0.570 nm, b = 1.419 nm, and c = 0.503 nm in space group *Pcan* (No. 60). The results of X-ray diffraction measurement supported the DTA observation (Fig. 4.1) that $MgNb_2O_6$ is formed at approximately 1000-1100 °C, in good agreement with other workers.[20,115,116]

Having established the optimum calcination temperature, alternative dwell times ranging from 1 h to 4 h with constant heating/cooling rates of 20 °C/min were applied at 1100 °C, as shown in Fig. 4.3. It is observed that the single phase of columbite-like $MgNb_2O_6$ (yield of 100% within the limitations of the XRD technique) was found to be possible only in powders, calcined at 1100 °C with dwell time of 3 h or more. The appearance of Nb_2O_5 phase (●) indicated that full crystallization have not occurred at relatively shorter calcination times.

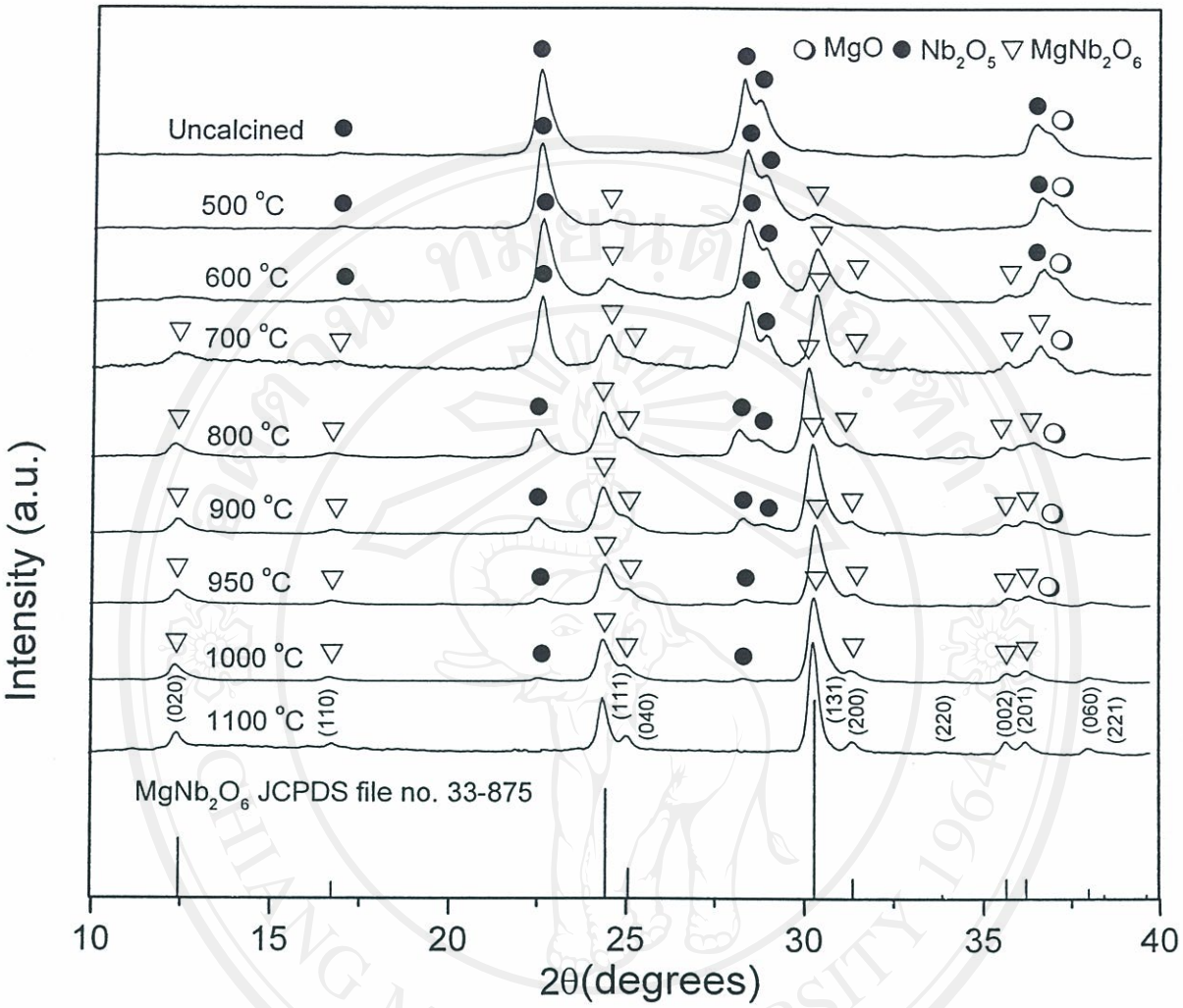

Fig. 4.2 XRD patterns of $MgNb_2O_6$ powder calcined at various temperatures for 3 h with heating/cooling rates of 20 °C/min.

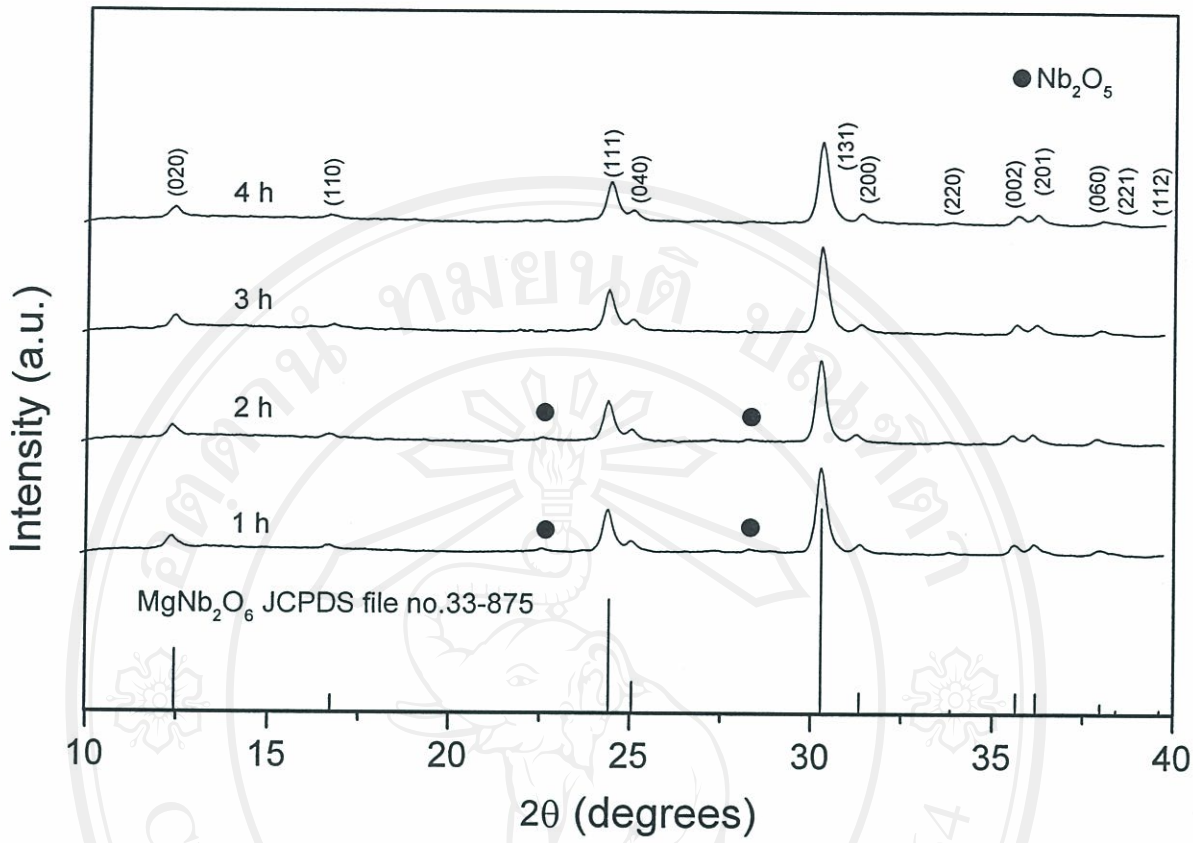

Fig. 4.3 XRD patterns of $MgNb_2O_6$ powder calcined at 1100 °C with heating/cooling rates of 20 °C/min for various dwell times.

Apart from the calcination temperature and dwell time, the effect of heating/cooling rates on the formation behaviour of $MgNb_2O_6$ was also investigated. Five heating/cooling rates (3, 5, 10, 15 and 20 °C/min) were selected for calcination condition of 1100 °C/3 h (Fig. 4.4). In this connection, it is shown that the yield of $MgNb_2O_6$ phase did not vary significantly with heating/cooling rates, indicating that fast heating/cooling rates can be employed for the preparation of $MgNb_2O_6$ phase. The experimental work carried out here suggests that the optimal calcination conditions for single phase $MgNb_2O_6$ is 1100 °C for 3 h with heating/cooling rates as fast as 20 °C/min, in agreement with literature.[20,23]

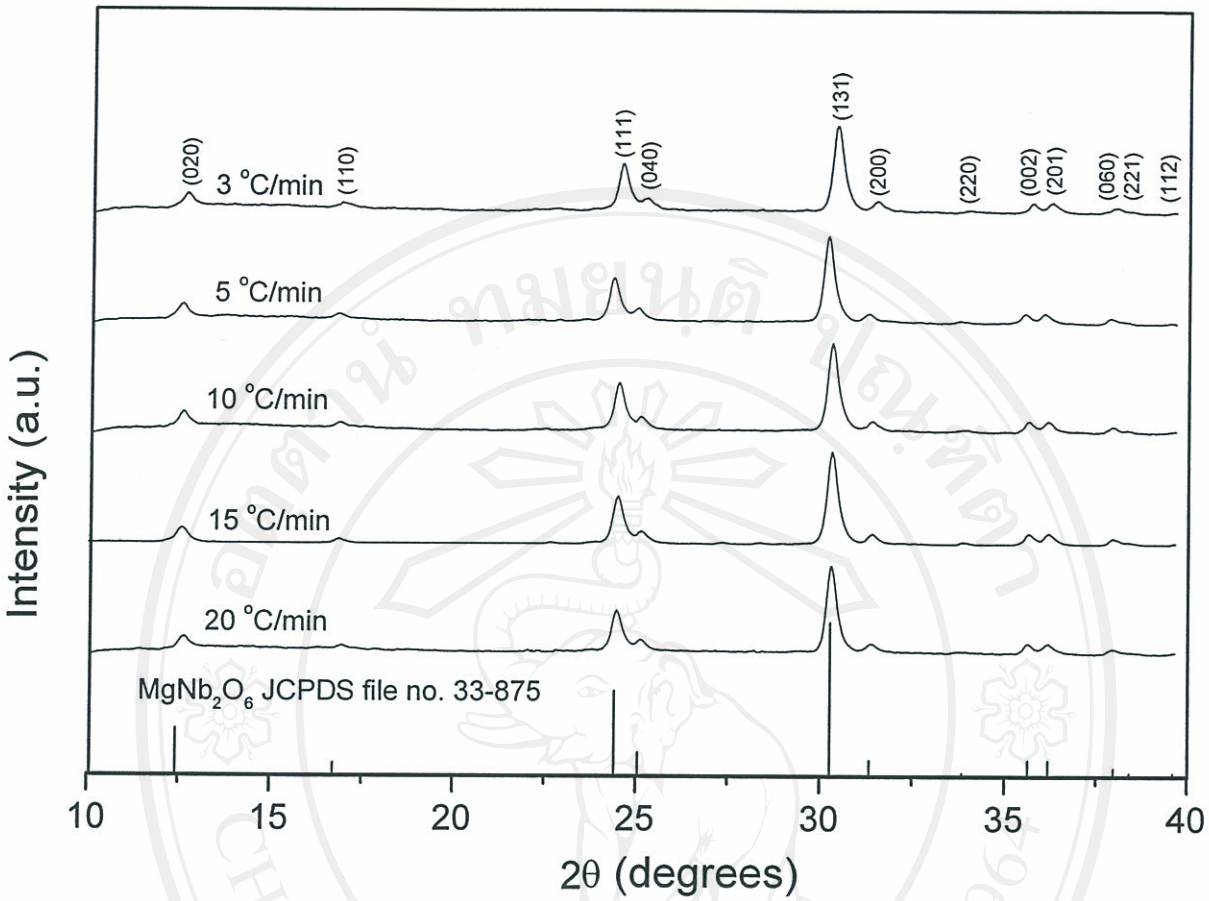

Fig. 4.4 XRD patterns of $MgNb_2O_6$ powder calcined at 1100 °C for 3 h with various heating/cooling rates.

.

4.1.1.3 Morphological analysis

The morphological evolution during calcination was investigated by scanning electron microscopy (SEM). Micrographs of the $MgNb_2O_6$ powders calcined at 1100 °C for 3 and 4 h with various heating/cooling rates from 3 to 20 °C/min are shown in Fig. 4.5 (a-d). In general, the particles are agglomerated and basically irregular in shape, with a substantial variation in particle size, particularly in samples calcined for longer dwell time or with faster heating/cooling rates.

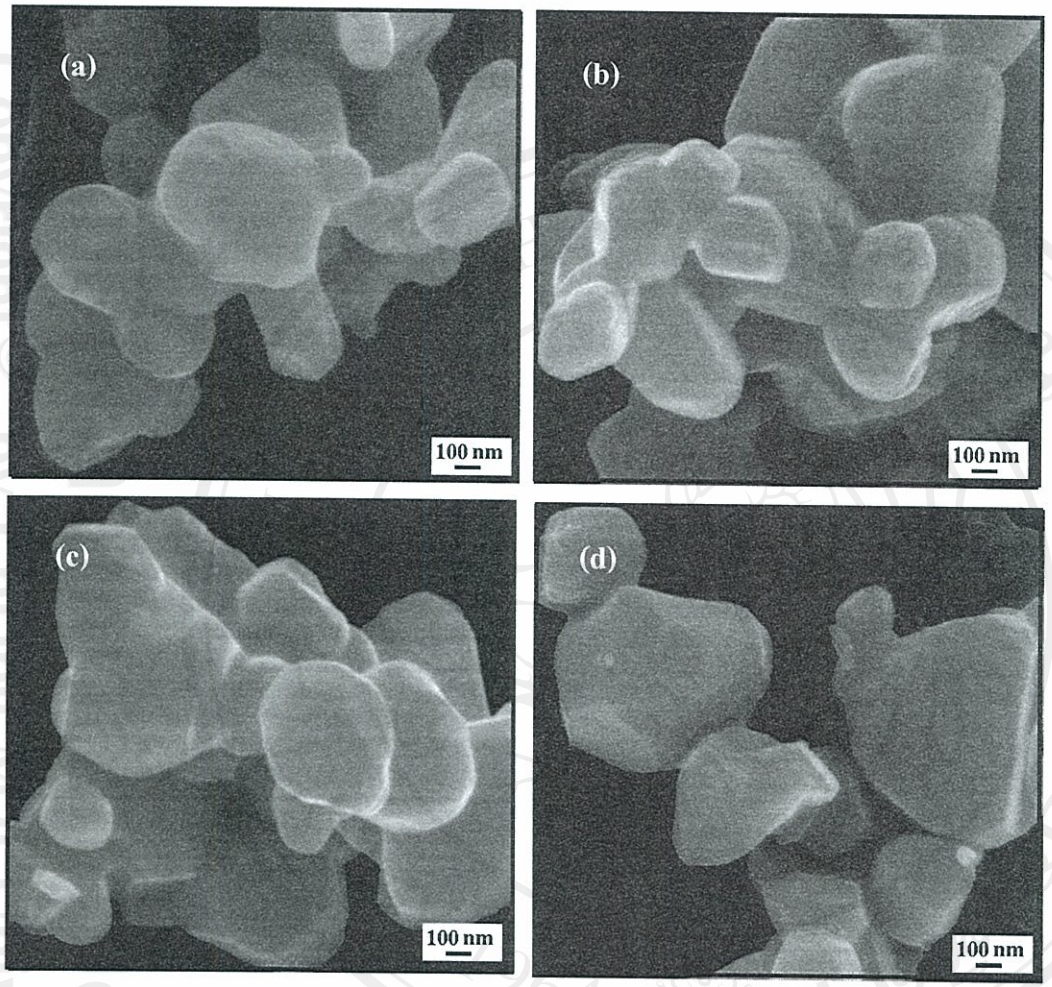

Fig. 4.5 SEM micrographs of the $MgNb_2O_6$ powders calcined at 1100 °C/3 h, with heating/cooling rates of (a) 3 °C/min, and (b) 10 °C/min, and calcined at (c) 1100 °C/3 h and (d) 1100 °C/4 h, both with heating/cooling rates of 20 °C/min.

4.1.2 Lead magnesium niobate powders

Having prepared the single-phase $MgNb_2O_6$ powder, a mixed oxide synthetic route was developed for the preparation of lead magnesium niobate powder. In this study, the phase formation, morphology and particle size of PMN has been investigated as a function of calcination conditions by TG-DTA, XRD and SEM techniques.

4.1.2.1 Thermal analysis

The TG and DTA curves recorded at a heating rate of 10 °C/min in air for an equimolar mixture of PbO and $MgNb_2O_6$ are given in Fig. 4.6. It is seen that TG curve demonstrates two distinct weight loss below 400 °C. The first weight loss occurs below 200 °C and the second one above 220 °C. In the temperature range from room temperature to ~ 250 °C, the sample shows small exothermic peak in the DTA curve at 250 °C, which are related to the second weight loss. This DTA peak can be attributed to the decomposition of organic species from the milling process. After the first weight loss, the sample shows a sharp fall in specimen weight with increasing temperature from 240-300 °C.

Corresponding to the second fall in specimen weight (~ 0.8 %), by increasing the temperature up to ~ 600 °C, the solid-state reaction occurs between PbO and $MgNb_2O_6$. The broad exothermic characteristic in the DTA curve represents that reaction, which has a maximum at ~ 600 °C. Moreover, another exothermic peaks with maximum at 800 °C was also observed in this profile. These temperatures have been obtained from the calibration of the sample thermocouple. It is to be noted that there is no obvious interpretation of the peaks, although it is likely to correspond to a phase transition reported by a number of researchers.[20,23]

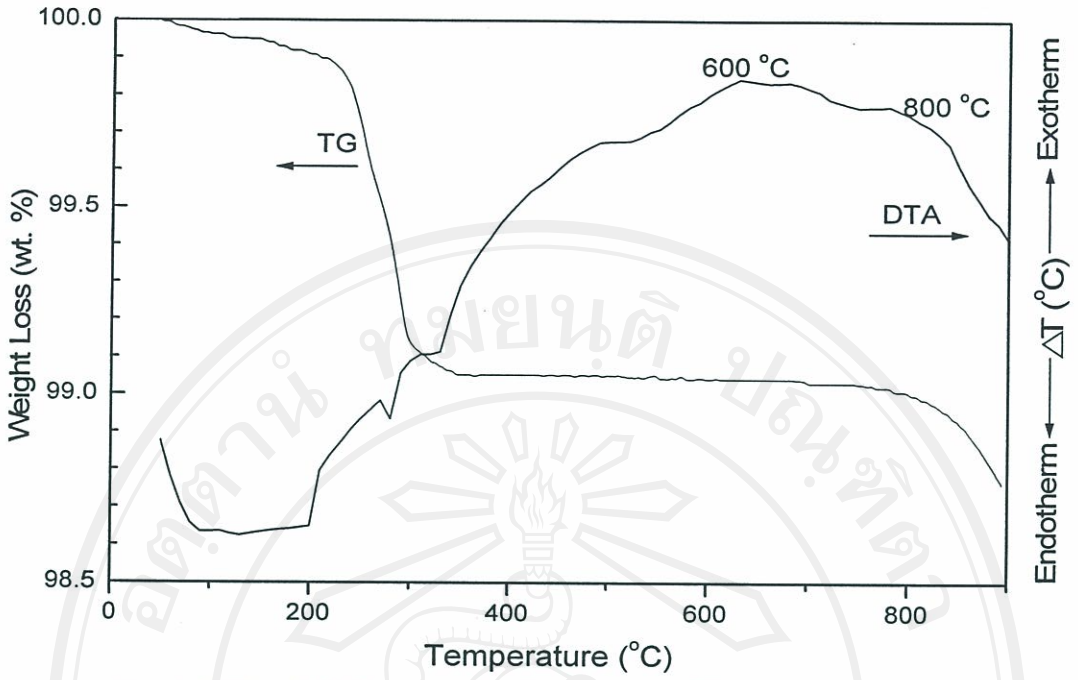

Fig. 4.6 TG and DTA curves for the mixture of PbO- $MgNb_2O_6$ powders.

4.1.2.2 Phase analysis

All calcined powders, together with that of the starting powder mixtures were examined by XRD in order to investigate the phase development (Figs. 4.7-4.9). As shown in Fig. 4.7, for the uncalcined powder and the powder calcined at 550 °C, only X-ray peaks of precursors PbO and $MgNb_2O_6$ are present, indicating that no reaction was yet triggered during the vibro-milling or low firing processes. The formation of pyrochlore phase, $Pb_3Nb_4O_{13}$ (▼) earlier reported by many researchers[7,20,21] has been found at 600 °C, which is associated to the second DTA exothermic effect in Fig. 4.6. This phase has a cubic structure (JCPDS file no. 25-443),[117] with cell parameter a = 1.056 nm in space group *Fd3m* (no. 227). It is seen that fine PMN crystallites were developed in the powder at a calcination temperature as low as 600 °C. The results of X-ray diffraction measurement supported the DTA observation (Fig. 4.6) that $Pb(Mg_{1/3}Nb_{2/3})O_3$ is formed at approximately 600-850 °C. In general, the strongest reflections apparent in the majority of this XRD pattern indicate the formation of the lead magnesium niobate,

$Pb(Mg_{1/3}Nb_{2/3})O_3$ (▽). These can be matched with JCPDS file number 27-1199 for the cubic phase, in space group *Pm3m* with cell parameters $a = 405$ pm.[118]

Depending on the calcination conditions, at least three minor phases were identified, i.e. PbO (○), $MgNb_2O_6$ (●), and $Pb_3Nb_4O_{13}$ (▼), which can be correlated with JCPDS files numbers 77-1971, 38-875 and 25-433, respectively. Unreacted PbO and $MgNb_2O_6$ phases are detected from the original mixture up to 600 °C, whereas minor amount of $Pb_3Nb_4O_{13}$ is observed at 600 °C and totally disappeared at higher temperature. By increasing the calcination temperature from 600 to 900 °C, the yield of the cubic PMN phase increase significantly until at 800 °C, a single phase of $Pb(Mg_{1/3}Nb_{2/3})O_3$ is formed. This study also shows that crystalline cubic PMN is the only detectable phase in the powder, after calcination in the range 800 to 900 °C. It is to be noted that a large temperature decrease observed at temperature greater than 850 °C in the DTA curve may be attributed to the PbO volatilisation, in consistent with other work.[23,40,119,120]

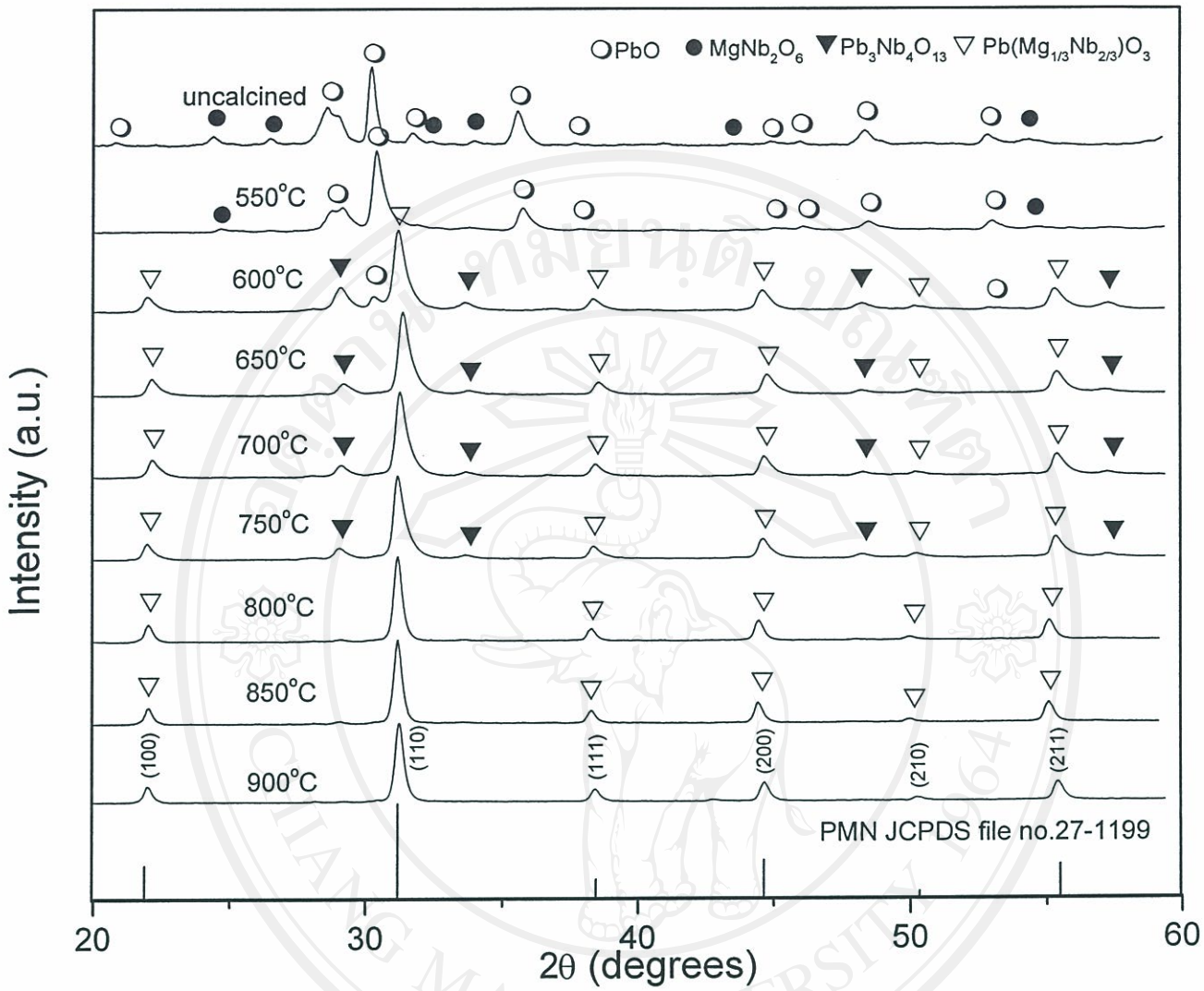

Fig. 4.7 XRD patterns of PMN powder calcined at various temperatures for 1 h with heating/cooling rates of 20 °C/min.

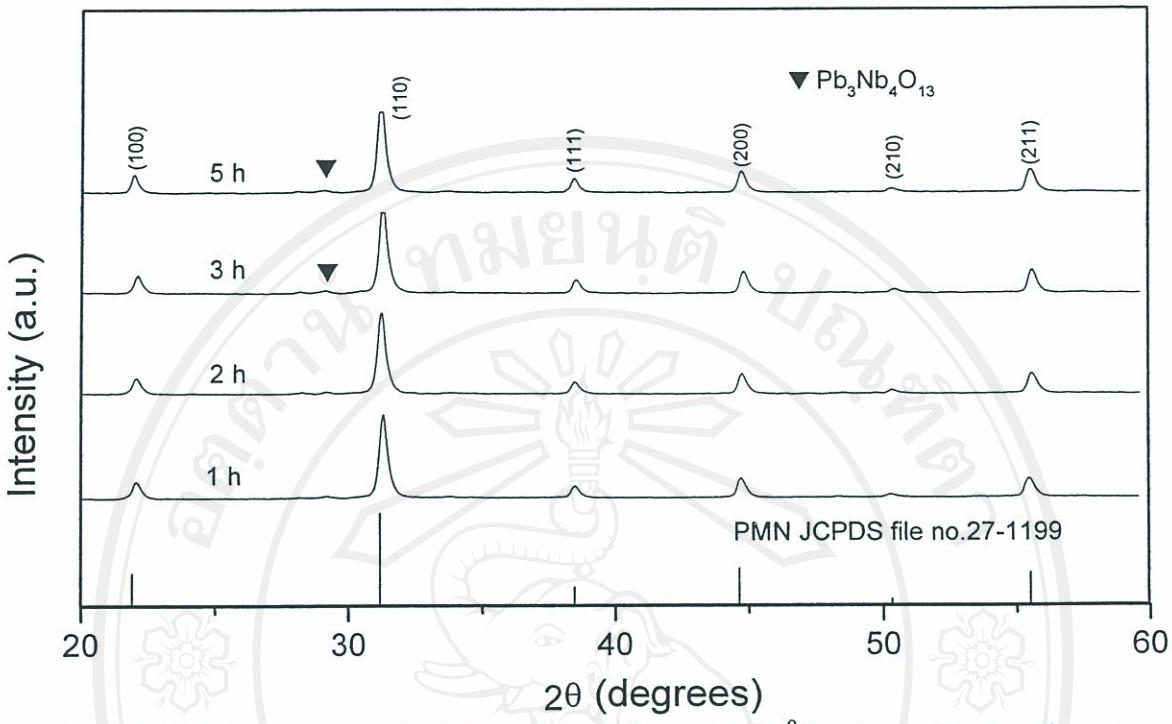

Fig. 4.8 XRD patterns of PMN powder calcined at 800 °C with heating/cooling rates of 20 °C/min for various dwell times.

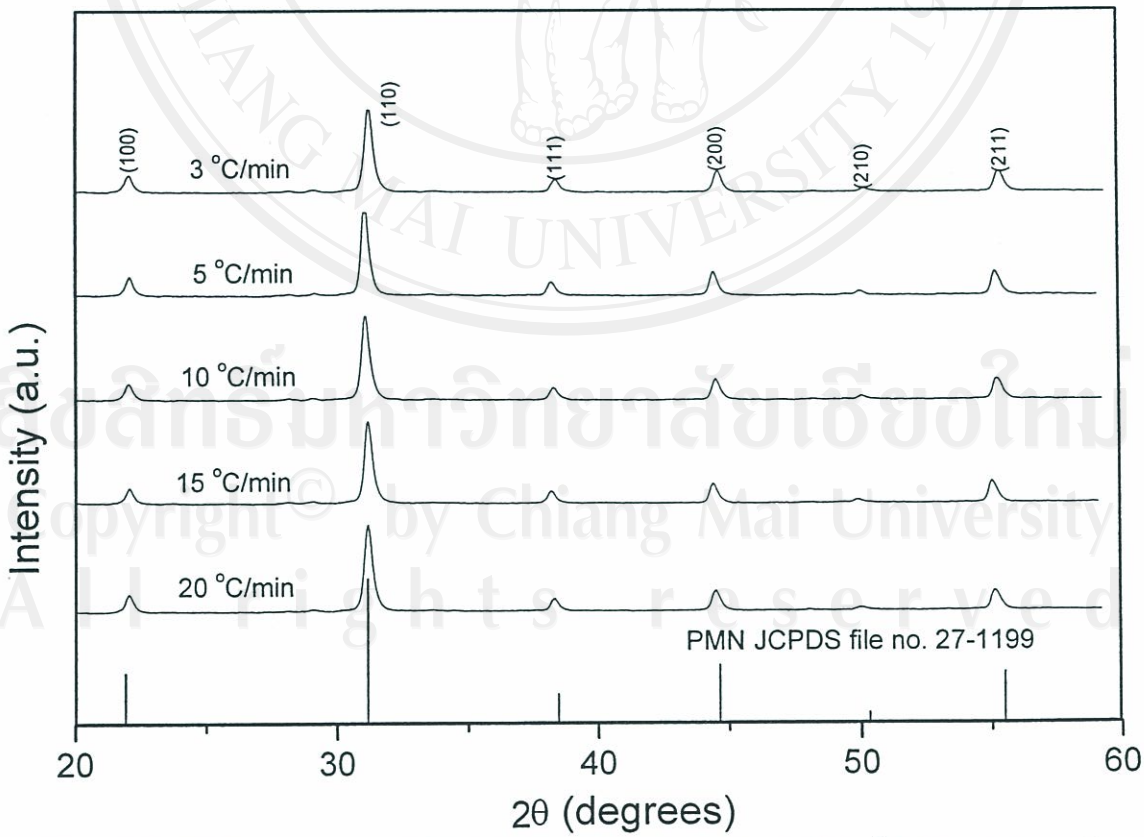

Fig. 4.9 XRD patterns of PMN powder calcined at 800 °C for 1 h with various heating/cooling rates.

Having established the optimum calcination temperature, alternative dwell times ranging from 1 to 5 h with constant heating/cooling rates of 20 °C/min were applied at 800 °C, as shown in Figs. 4.8 and 4.9, respectively. In Fig. 4.8, the single phase of perovskite PMN (yield of 100% within the limitations of the XRD technique) was found to be possible in powders, calcined up to 800 °C with dwell time of 1 h or 2 h. However, for prolong times the appearance $Pb_3Nb_4O_{13}$ phase indicated that full crystallization have not occurred at relatively longer calcination times. However, in the work reported here, it is to be noted that single–phase of PMN powder was also successfully obtained for a calcination temperature of 800 °C with dwell time of 1 h applied (Fig. 4.8). This is probably due to the effectiveness of vibro-milling and a carefully optimised reaction. The observation that the dwell time effect may also play an important role in obtaining a single-phase perovskite product is also consistent with other similar systems.[15,16]

Apart from the calcination temperature and dwell time, the effect of heating/cooling rates on the formation behaviour of PMN was also investigated. Five heating/cooling rates (3, 5, 10, 15 and 20 °C/min) were selected for calcination condition of 800 °C/1h (Fig. 4.9). In this connection, it is shown that the yield of PMN phase did not vary significantly with heating/cooling rates, indicating that fast heating/cooling rates can leads to full crystallization of PMN phase without time for the formation of pyrochlore phase or lead vaporization. The observation that faster heating/cooling rates are required for lead-based ferroelectrics is also consistent with other investigators.[145-146]

Based on the DTA and XRD data, it may be concluded that, over a wide range of calcination conditions, single phase PMN cannot be straightforwardly formed via a solid state mixed oxide synthetic route. The experimental work carried out here suggests that the optimal calcination conditions for single phase PMN is 800 °C for 1 with heating/cooling rates as fast as 20 °C/min which is closed to that of Ananta *et al.*[23] (~ 800 °C for 3 h).

4.1.2.3 Morphological analysis

The morphological changes in the PMN powders formed by a mixed oxide technique are shown in Fig. 4.10 (a-d) as a function of the formation temperature. After various calcination conditions, the powders have similar morphology. They had spherical secondary particles (0.5-2.2 μm) composed of nanosized primary particulates (150-560 nm). In general, this granule characteristic will offer an apparent advantage towards achieving a high sintered density and homogeneous microstructure for PMN ceramic at a reduced sintering temperature.

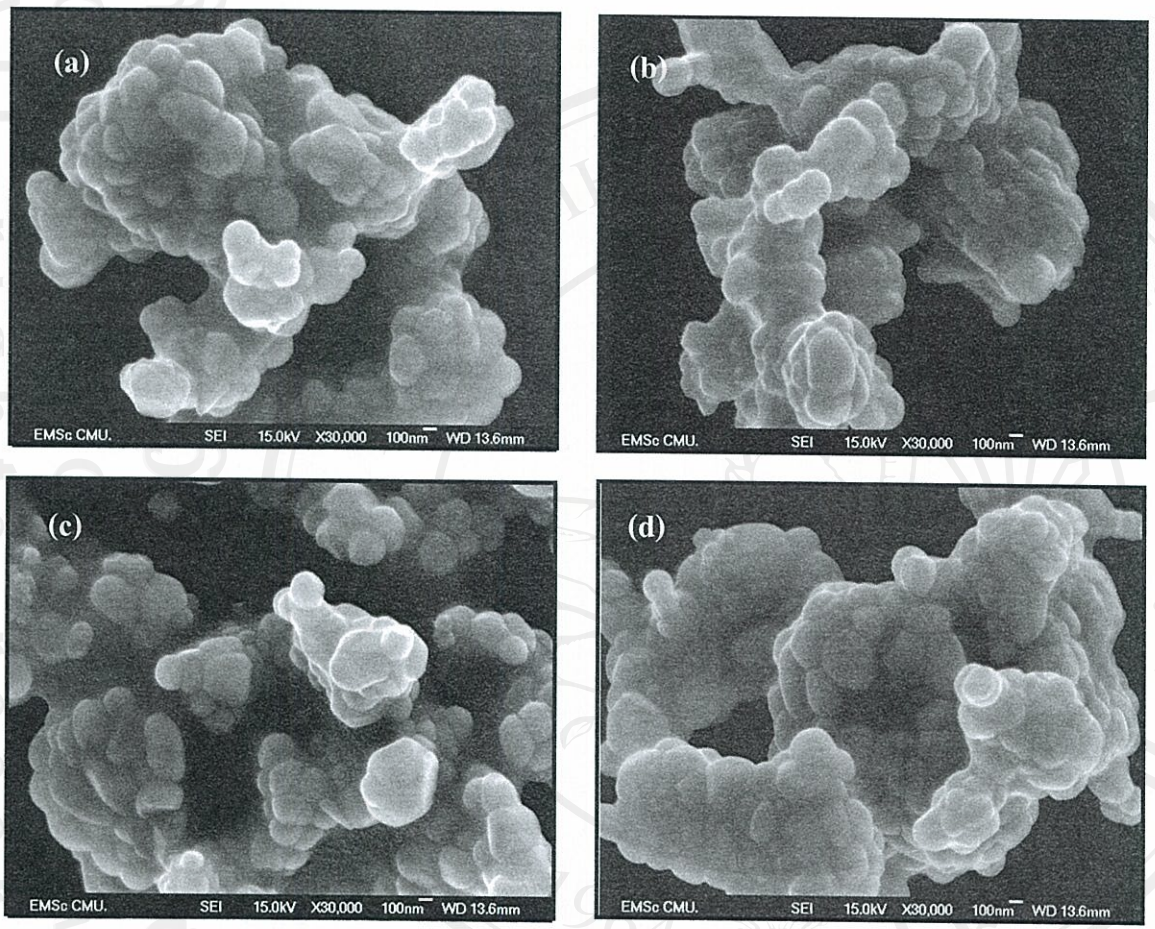

Fig. 4.10 SEM micrographs of the PMN powders calcined at 800 °C/1 h, with heating/cooling rates of (a) 5 °C/min and (b) 20 °C/min, and calcined at (c) 800 °C/2 h and (d) 900 °C/1 h, both with heating/cooling rates of 20 °C/min.

4.1.3 Lead Magnesium Niobate Ceramics

4.1.3.1 Phase analysis

X-ray diffraction patterns of PMN ceramics formed at various sintering conditions are given in Figs. 4.11-4.13. The strongest reflections in the majority of the XRD patterns indicate formation of the perovskite phase of $Pb(Mg_{1/3}Nb_{2/3})O_3$, which could be matched with JCPDS file no. 27-1199.[118] To a first approximation, this phase has a cubic perovskite-type structure in space group *Pm3m* (no. 221), with cell parameter a = 405 pm. However, some additional reflections, which correlate with a pyrochlore phase of composition $Pb_3Nb_4O_{13}$ (JCPDS file no. 25-443),[117] are found in some XRD patterns (at $2\theta \sim 29.256^{\circ}$, $33.928^{\circ}$and 48.761°). This phase has a cubic structure, with cell parameter a = 1.056 nm in space group *Fd3m* (no. 227). For the purposes of estimating the concentrations of pyrochlore phase present, eqn (3.4) has been applied to the diffraction patterns obtained, as given in Table 4.1. It should be noted that no evidence of pyrochlore phases $Pb_2Nb_2O_7$, $Pb_3Nb_2O_8$ and $Pb_5Nb_4O_{15}$ reported by other worker[18-20] has been formed here.

The effect of sintering temperature in the range from 1200 to 1240 °C for 2 h with heating/cooling rates of 5 °C/min on phase formation was found to be insignificant, with a single phase of perovskite PMN (yield of 100% within the limitations of the XRD technique) obtained in all cases. This is probably due to a combination of the carefully optimised reaction to form single-phase precursor powders[15,17,18] and the refined sintering procedure. However, (as shown in Table 1), pyrochlore phase (~ 5.11-6.43 wt%) was found to coexist with the perovskite phase in PMN sintered at 1265 °C and 1280 °C. These pyrochlore formations could be attributed to many factors, including PbO evaporation.

Having established the optimum sintering temperature, alternative dwell times of 0.5, 2, 4 and 8 h with constant heating/cooling rates of 5 °C/min were applied at 1240°C, as shown in Fig. 4.12. It is seen that the single phase of perovskite PMN

was found to be possible only in ceramics, sintered at 1240 °C with dwell time of 2 h or less. The appearance of pyrochlore $Pb_3Nb_4O_{13}$ indicated that PbO volatilization have occurred at prolong heating times.

Apart from the sintering temperature and dwell time, the effect of heating/cooling rates on the formation behavior of PMN was also investigated. Five heating/cooling rates (1, 3, 5, 15 and 30 °C/min) were selected for sintering condition of 1240 °C/2 h (Fig. 4.13). In this connection, it is shown that the yield of PMN phase was improved significantly by increasing the heating/cooling rates. The single phase of perovskite PMN was found to be possible only in sample sintered at 1240 °C with heating/cooling rates of 5 °C/min or faster, in consistent with other workers.[121] This observation reveals that faster heating/cooling rates are required for lead-based ferroelectrics because the faster rates can lead to single-phase PMN without time for the formation of pyrochlore phase or lead vaporization.

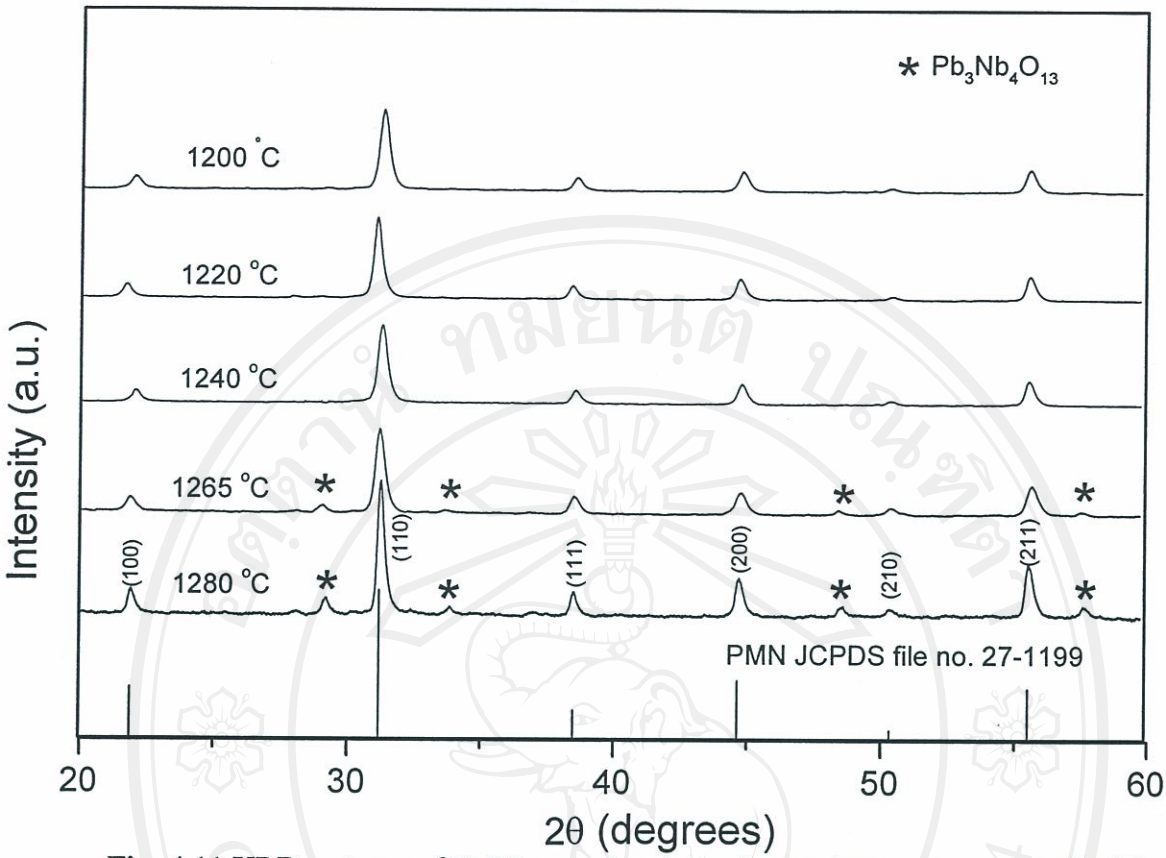

Fig. 4.11 XRD patterns of PMN ceramics sintered at various temperatures for 2 h with heating/cooling rates of 5 °C/min.

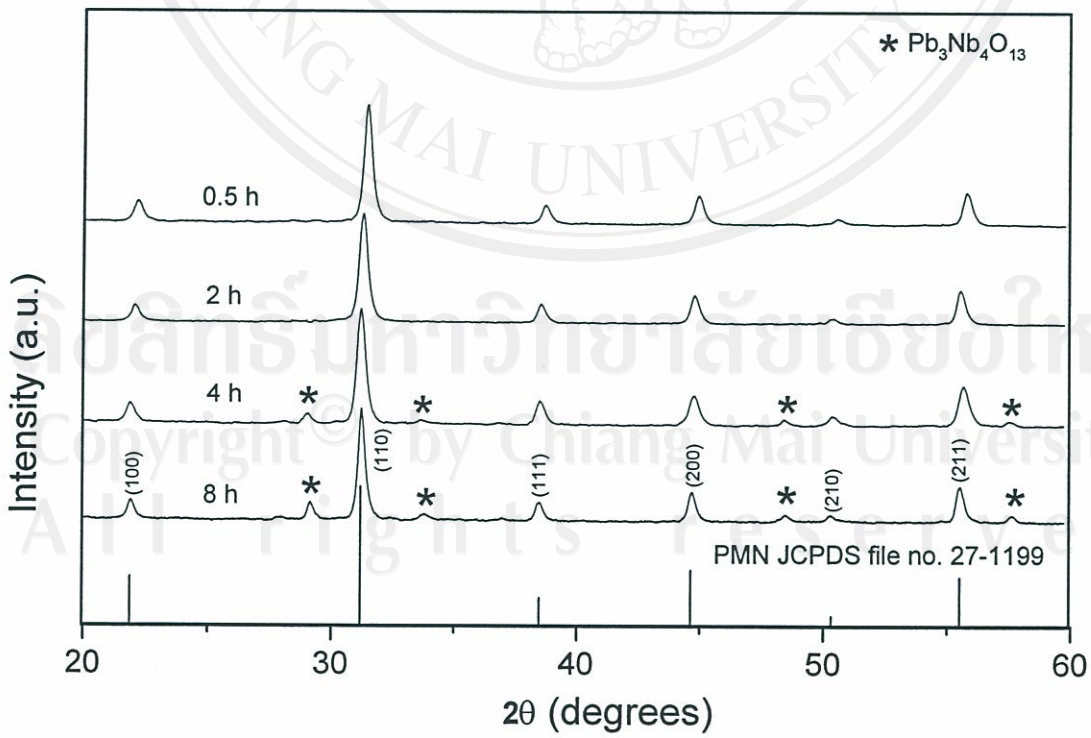

Fig. 4.12 XRD patterns of PMN ceramics sintered at 1240 °C with heating/cooling rate of 5 °C/min for various dwell times.

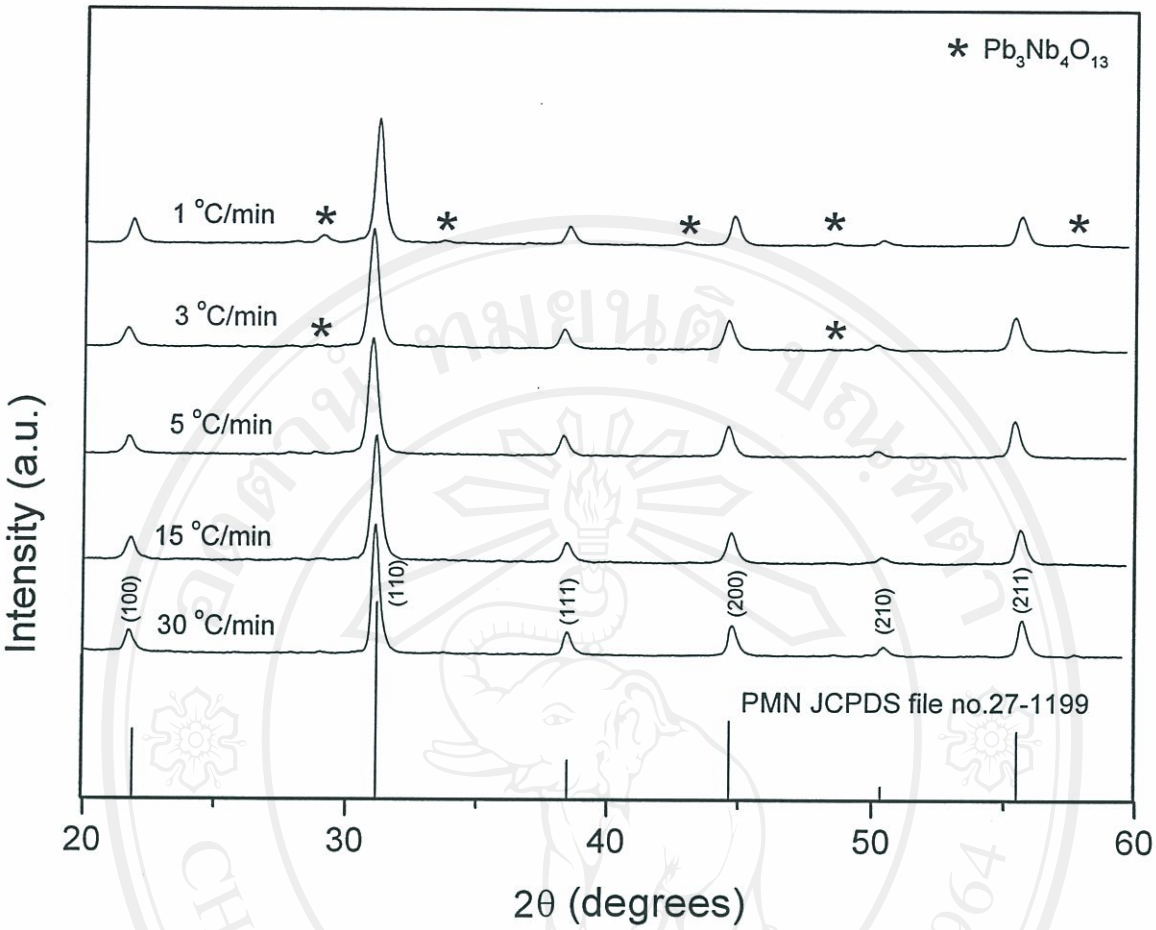

Fig. 4.13 XRD patterns of PMN ceramics sintered at 1240 °C for 2 h with various heating/cooling rates.

4.1.3.2 Densification analysis

The theoretical density of cubic phase of PMN ceramics, which was used for the relative density calculations in the sintered samples, was estimated from the lattice parameter data to be ~ 8.144 g/ cm^3(JCPDS file no. 27-1199).[118] D ensities of the sintered samples were determined by using Archimedes principle.

Density, shrinkage and weight loss data of all PMN ceramics sintered at various conditions are given in Table 4.1. It is observed that a density of about 89-96% of the maximum value for PMN can be achieved in this study (Fig. 4.14). The maximum density was obtained only in the samples sintered at 1240 °C for 2 h with heating/cooling rates of 5 °C/min. From Fig. 4.14, the observed fall-off in density at higher temperature is probably due both to PbO loss impeding the sintering process and the lower density of the pyrochlore phase, which is present with a concentration of ~ 5-6 wt%, in consistent with other work.[16] The effect of dwell times on density of PMN ceramics sintered at 1240 °C with heating/cooling rate of 5 °C/min are shown in Fig. 4.15. Density increases as dwell time increase from 0.5 h to 2 h and decreases at higher dwell time. Apart from the sintering temperature and dwell time, the effect of heating/cooling rates on the densification was also investigated. It is seen that density increases as the rate increases from 1 to 5 °C/min and stables at higher rates (Fig. 4.16).

Shrinkage and weight losses data of all samples sintered at various conditions are illustrated in Figs. 4.17- 4.19. The change in dimension was rapidly increased with sintering temperature at 1220 °C to 1240 °C and nearly constant after 1240 °C (Fig. 4.17). It is seen that an increase in sintering temperature and dwell time resulted in an increase in linear shrinkage (Figs. 4.17 and 4.18, respectively). Whereas, in term of the effect of heating/cooling rates, it is seen that shrinkage increase as the rate increases from 1 to 5 °C/min and decreases at higher rates (Fig. 4.19).

Weight losses of all PMN ceramics during sintering procedure can be thought of as a measure of the degree of PbO volatilization. This was analyzed by recording

the weight before and after sintering procedure. In general, the weight loss increases with sintering temperature and dwell times but did not vary significantly with heating/cooling rates (except at rates 1 °C/min), in consistent with the densification result. It is interesting to note that when heating/cooling rates of 1 °C/min was applied to the samples sintered at 1240 °C for 2 h (Fig. 4.19), significant weight loss of about 9% was observed. This result also confirms that the slower rates can provide enough time for occurring of lead volatilization and result in the formation of pyrochlore as shown in Fig. 4.13.

Table 4.1 Phase formation and densification of PMN ceramics sintered at various conditions.

Sintering temperature (°C)	Dwell times (h)	Heating/cooling rates (°C/min)	Perovskite phase (wt%)	Pyrochlore phase (wt%)	Relative density* (%)	Shrinkage** (%)	Weight*** loss (%)
1200	2	5	100.00	0.00	88.98	7.44	8.33
1220	2	5	100.00	0.00	91.51	7.61	10.00
1240	2	1	95.87	4.13	93.83	13.30	20.83
1240	2	3	97.16	2.84	94.57	13.37	12.41
1240	2	5	100.00	0.00	96.43	13.44	12.50
1240	2	15	100.00	0.00	96.26	13.41	12.42
1240	2	30	100.00	0.00	95.20	13.50	13.15
1240	0.5	5	100.00	0.00	90.82	12.64	8.75
1240	4	5	95.18	4.82	94.71	13.46	14.30
1240	8	5	92.04	7.96	92.85	13.79	17.50
1265	2	5	94.89	5.11	94.42	13.82	15.00
1280	2	5	93.57	6.43	92.99	13.73	17.91

* The estimated precision of the relative density is ± 0.6 %

** The estimated precision of shrinkage is ± 0.7 %

*** The estimated precision of weight loss is ± 1.0%

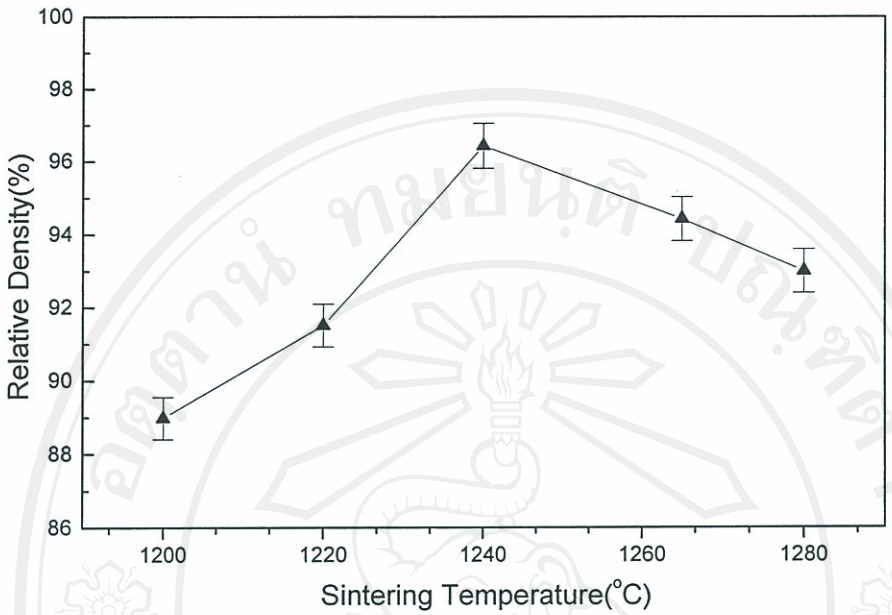

Fig. 4.14 Dependence of relative density in PMN ceramics sintered at various sintering temperatures.

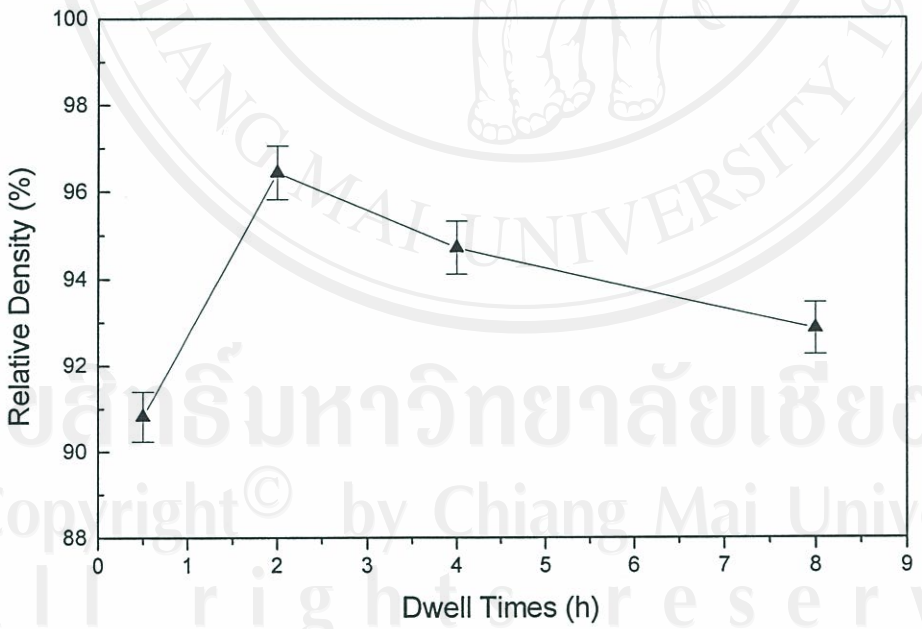

Fig. 4.15 Sintering density as a function of dwell times for PMN ceramics sintered at 1240 °C.

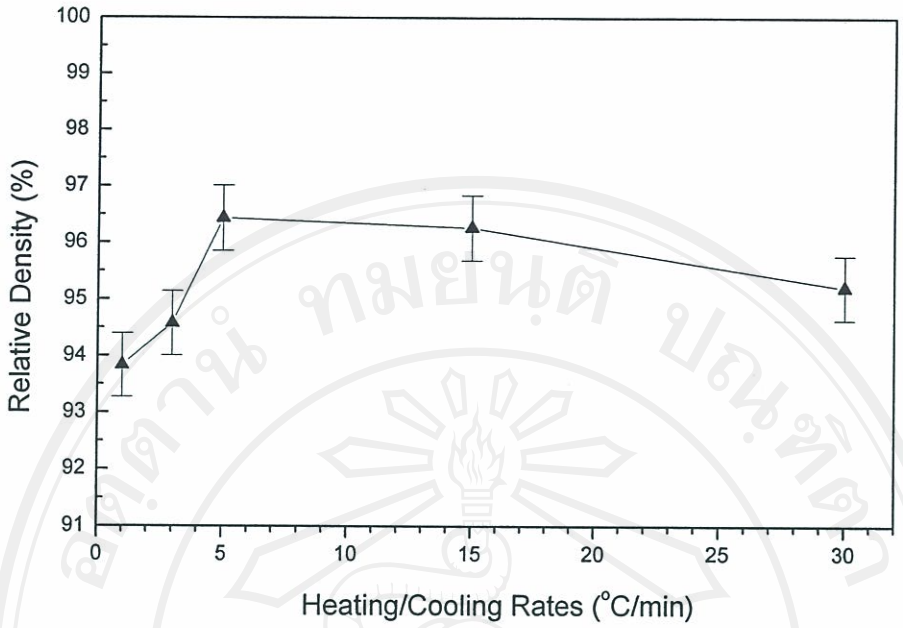

Fig. 4.16 Dependence of relative density on heating/cooling rates for PMN ceramics sintered at 1240 °C.

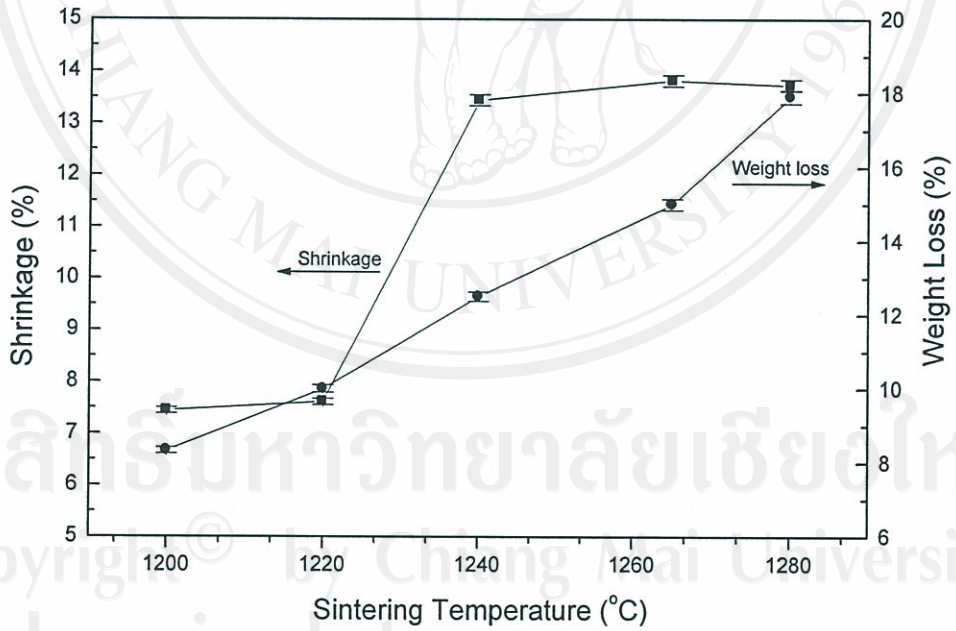

Fig. 4.17 Dependence of shrinkage and weight loss on sintering temperature for PMN ceramics.

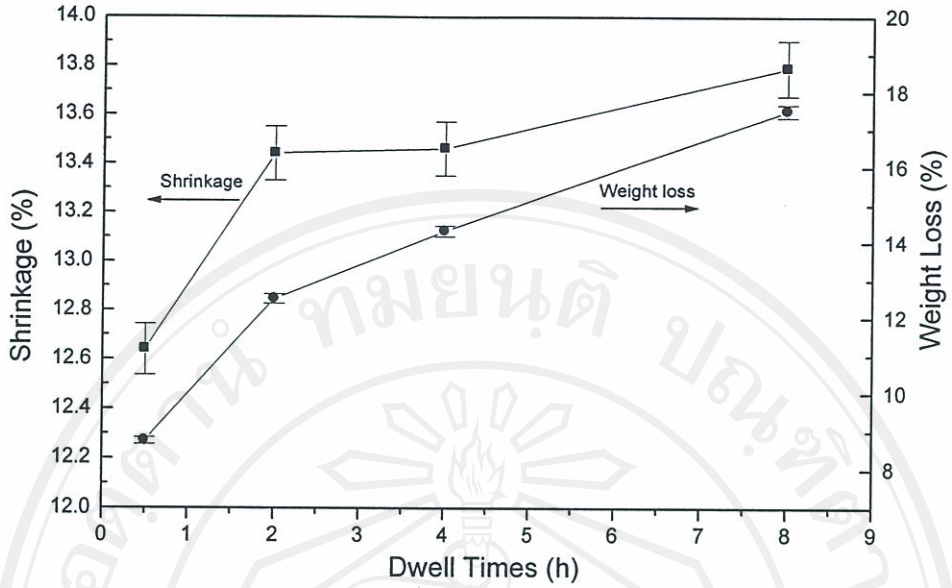

Fig. 4.18 Dependence of shrinkage and weight loss on dwell times for PMN ceramics sintered at 1240 °C.

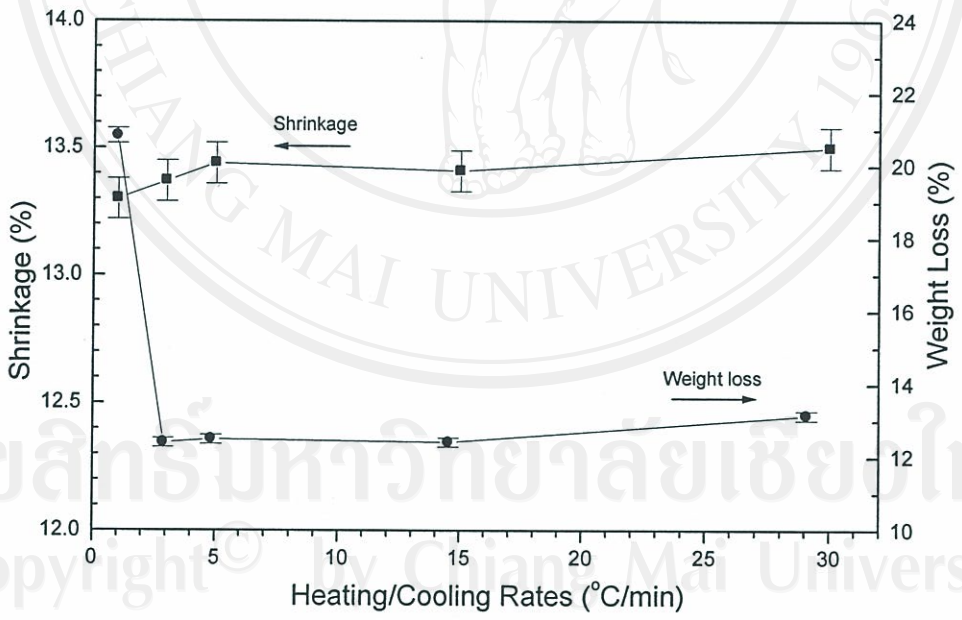

Fig. 4.19 Dependence of shrinkage and weight loss on heating/cooling rates for PMN ceramics sintered at 1240 °C.

4.1.3.3 Microstructural analysis

Microstructural development during sintering was investigated by scanning electron microscopy (SEM). Free and fracture surface micrographs of only some selected PMN ceramics are shown in Figs. 4.20-4.22 and Figs. 4.24-4.25, respectively. SEM micrographs of as-sintered ceramics showed few pores at grain boundaries and triple points; cracks or microcracks were not detected (Figs. 4.20-4.22). The effect of sintering conditions on grain size of the sintered samples are given in Table 4.2. The result indicates that grain size tends to increase with sintering temperature and dwell times, in agreement with other works.[23,24,28] However, average grain sizes of PMN ceramics did not vary significantly with heating/cooling rates. It should be noted that a distribution of the second phases (arrowed) over the PMN grains are found in some samples, especially when lower dwell time and heating/cooling rates were applied.

It was recognized that the XRD data alone could neither confirm nor rule out the presence of MgO because the high intensity XRD peak of MgO at d_{200} = 2.106 Å is almost overlapped by the perovskite PMN peak at d_{200} = 2.03 Å. Nevertheless, the presence of MgO in specimens was confirmed by SEM/EDX analysis. In general, EDX analysis of PMN grains showed that the composition (at%) of Pb : Mg : Nb is 17.75 : 6.65 : 18.14. MgO inclusions correspond to dark particles, which can be found on the surfaces of some PMN grains as shown in Figs. 4.21 (c) and (d), and 4.22 (d). Their corresponding EDX spectra are given in Fig. 4.25 where the composition (at%) of Pb : Mg : Nb is revealed as 3.34 : 34.95 : 2.49. The composition is deficient in Pb and Nb but rich in Mg, relative to MgO phase. It is to be note that the characteristic morphology of MgO dispersed in PMN grains is consistent with Guha.[122]

Table 4.2 Average grain sizes of PMN ceramics sintered at various conditions.

Temperature (°C)	Dwell times (h)	Heating/cooling rates (°C/min)	Average grain sizes* (μm)
1200	2	5	2.95
1240	2	5	4.56
1265	2	5	6.42
1240	2	1	4.40
1240	2	3	4.45
1240	2	15	4.80
1240	2	30	4.61
1240	0.5	5	2.34
1240	4	5	4.91
1240	8	5	7.12

*Values calculated by linear intercept technique and estimated precision of the grain sized is ± 1%

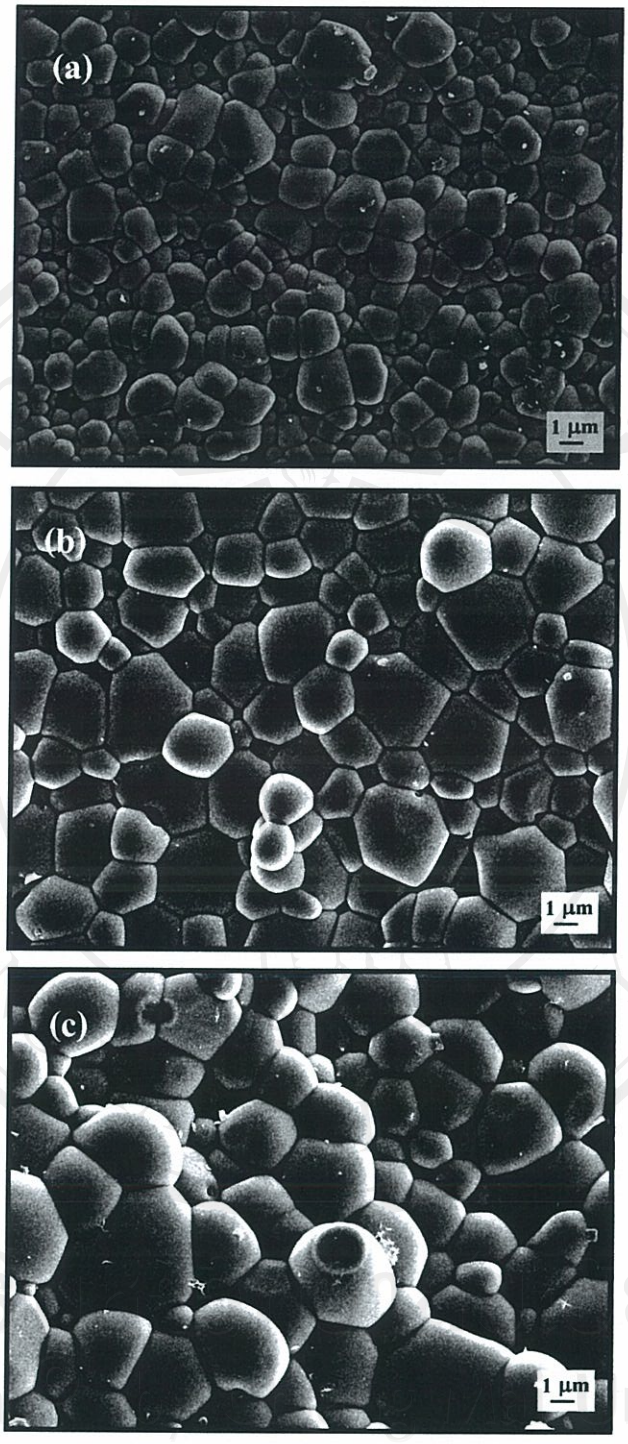

Fig. 4.20 SEM micrographs of free surfaces of PMN ceramics sintered at (a) 1200 °C, (b) 1240 °C and (c) 1265 °C, for constant dwell time of 2 h with heating/cooling rates of 5 °C/min.

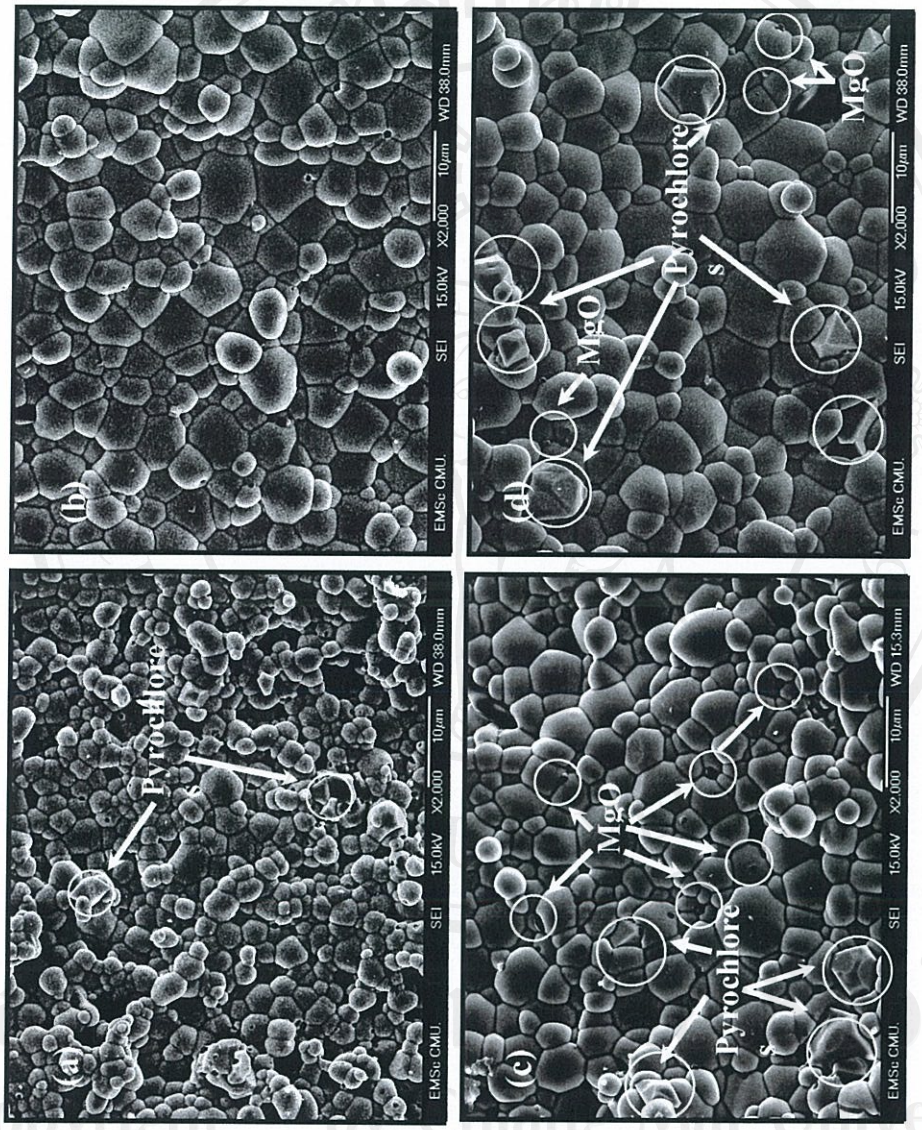

Fig. 4.21 SEM micrographs of free surfaces of PMN ceramics sintered at 1240 °C with heating/cooling rates of 5 °C/min for (a) 0.5, (b) 2, (c) 4 and (d) 8 h.

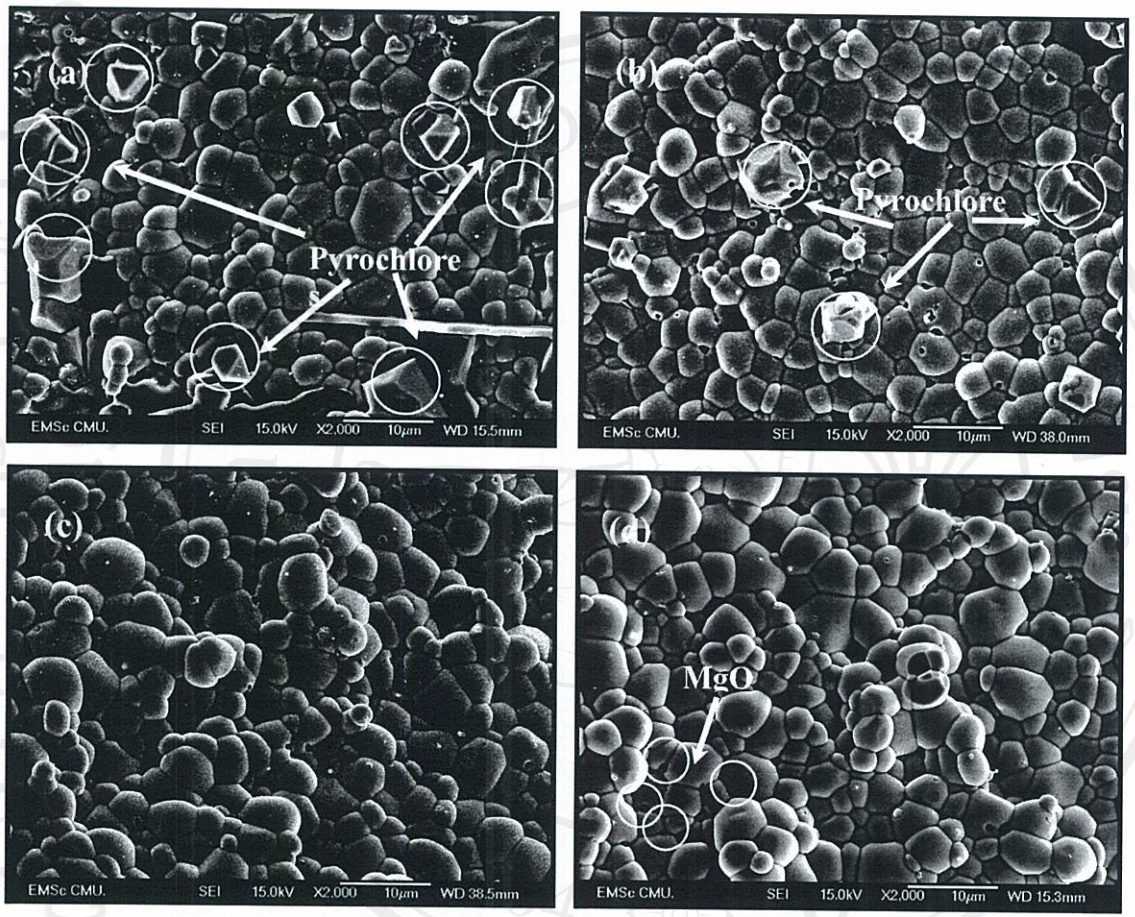

Fig. 4.22 SEM micrographs of free surfaces of PMN ceramics sintered at 1240 °C for 2 h with heating/cooling rates of (a) 1, (b) 3, (c) 15 and (d) 30 °C/min.

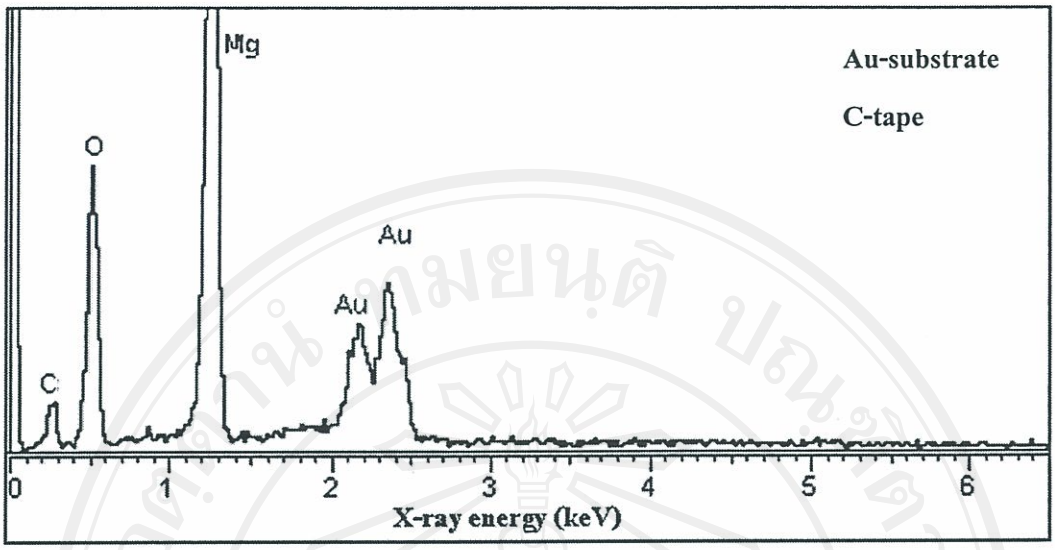

Fig. 4.23 Representative EDX spectra obtained from the dark particles exist on the surface of PMN grains (see Fig. 4.21 (c)).

The fracture surfaces of PMN ceramics sintered at various conditions are shown in Figs. 4.24 and 4.25. Some form of grain aggregates was found in the samples sintered for too short (Fig. 4.24 (a)) or too long (Fig. 4.24 (d)) dwell time, and also with slow heating/cooling rates of 1 °C/min (Fig. 4.25 (a)). It is to be noted that there is no obvious interpretation of grain aggregation, although it is likely to correspond to the influence of lead loss indicated by XRD and densification results reported in earlier sections (Figs. 4.12-4.13 and 4.15-4.16). On the other hand, the samples sintered with the rates of 3, 15 and 30 °C/min are of very similar grain appearance and exhibit typical microstructures of PMN ceramics.[123]

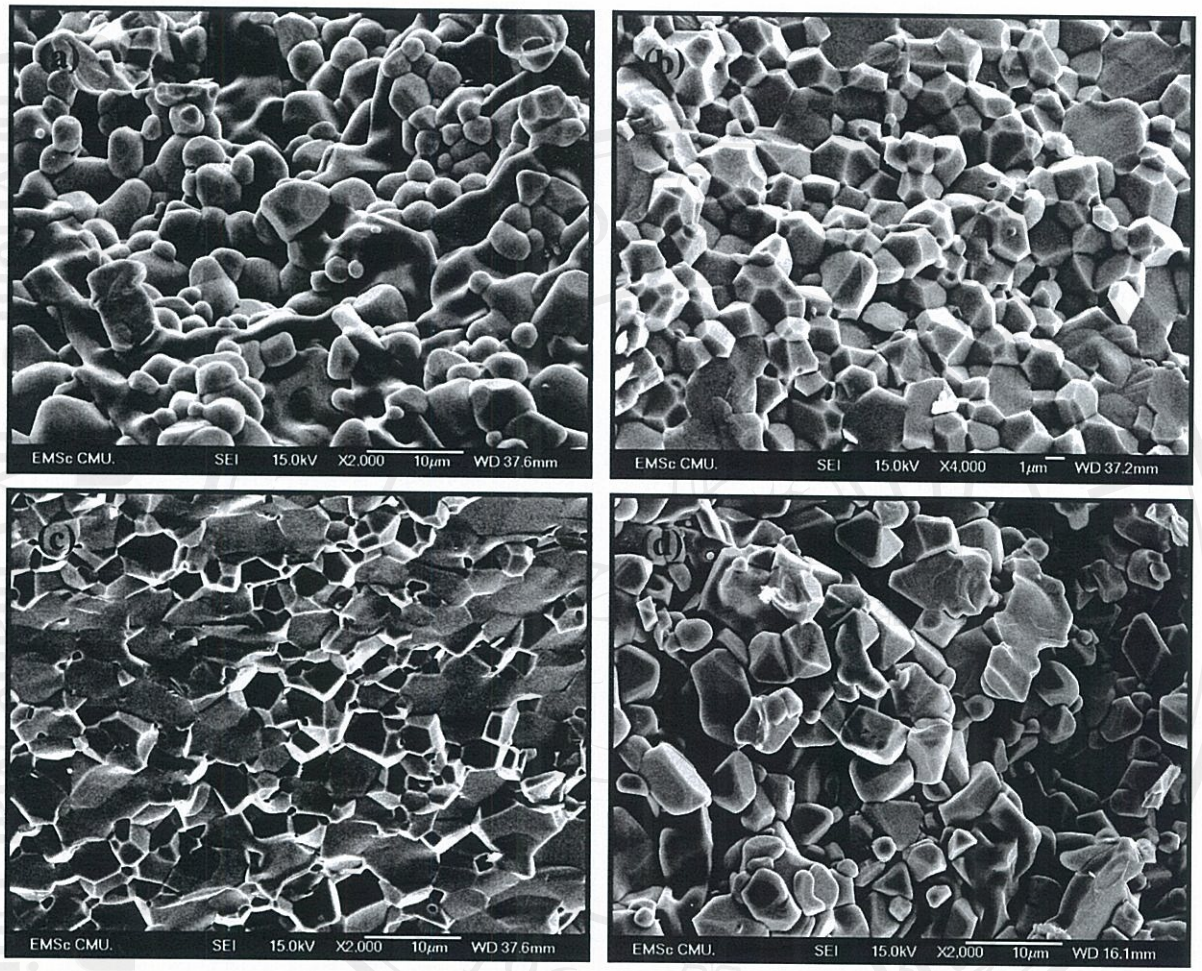

Fig. 4.24 SEM micrographs of fracture surfaces of PMN ceramics sintered at 1240 °C with heating/cooling rates of 5 °C/min for (a) 0.5, (b) 2, (c) 4 and (d) 8 h.

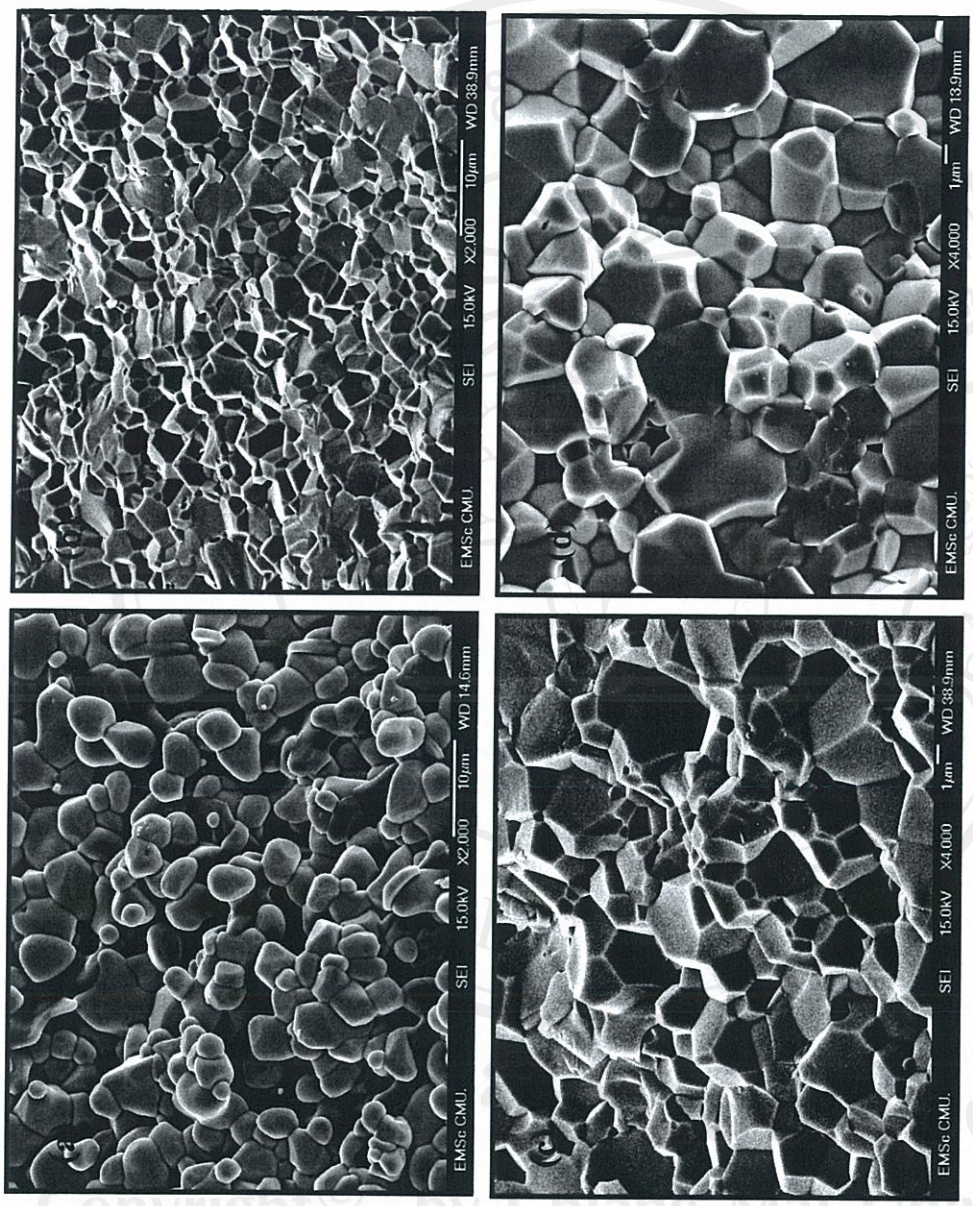

Fig. 4.25 SEM micrographs of fracture surfaces of PMN ceramics sintered at 1240 °C for 2 h with heating/cooling rates of (a) 1, (b) 3, (c) 15 and (d) 30 °C/min.

4.2 Lead Titanate (PT)

4.2.1 Lead titanate powders

4.2.1.1 Thermal analysis

DTA curve recorded at a heating rate of 10 °C/min in air for an equimolar mixture of lead oxide and titanium oxide is shown in Fig. 4.26. Three exothermic peaks are observed in the approximate range from 280 to 340 °C, 360 to 450 °C and 480 to 680 °C. These temperatures have been obtained from the calibration of the sample thermocouple. The first exothermic peak is believed to relate to the elimination of organic residuals from the rubber lining contamination during milling. However, it is to be noted that there is no obvious interpretation of the peaks after 340 °C, although it is likely to correspond to a phase transition reported by a number of workers.[40,45,48] These data were used to define the ranges of temperatures (400 to 800 °C) for XRD investigation.

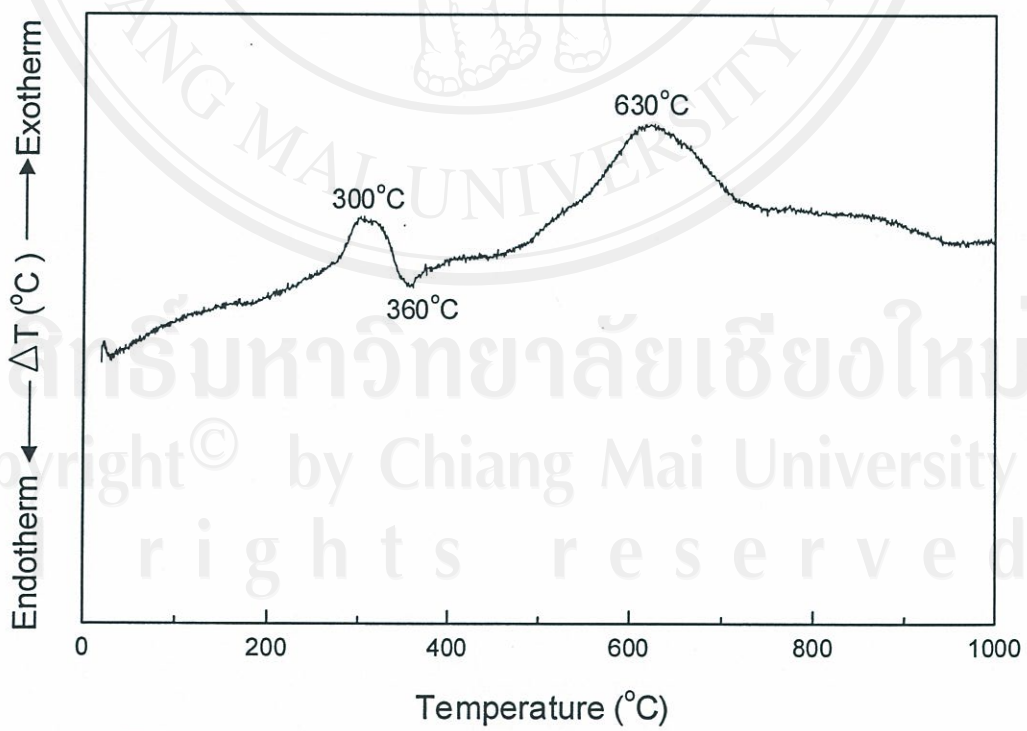

Fig. 4.26 A DTA curve for the mixture of PbO-TiO_2 powder.

4.2.1.2 Phase analysis

All calcined powders, together with that of the starting powder mixtures were examined by XRD in order to investigate the phase development (Figs. 4.27-4.31). As shown in Fig. 4.27, for the uncalcined powder and the powder calcined at 400 °C, only X-ray peaks of precursors PbO and TiO_2 are present, indicating that no reaction was yet triggered during the vibro-milling or low firing processes. The formation of lead deficient phase, $PbTi_3O_7$ (■) earlier reported by many researchers[16-17] has been found at 450 °C, which is associated to the second DTA exothermic effect in Fig. 4.26. This pyrochlore (or a metastable intermediate) phase has a monoclinic structure with cell parameter a = 107.32 pm, b = 381.2 pm, c = 657.8 pm and β = 98.08° (JCPDS file number 21-949).[124] It is seen that fine PT crystallites were developed in the powder at a calcination temperature as low as 500 °C.

The results of X-ray diffraction measurement supported the DTA observation (Fig. 4.27) that $PbTiO_3$ is formed at approximately 480-680 °C. In general, the strongest reflections apparent in the majority of this XRD pattern indicate the formation of the lead titanate, $PbTiO_3$ (○). These can be matched with JCPDS file number 6-452 for the tetragonal phase, in space group *P4/mmm* with cell parameters a = 389.93 pm and c = 415.32 pm.[125] Depending on the calcination conditions, at least three minor phases were identified, i.e. PbO (●), anatase-TiO_2 (*), and $PbTi_3O_7$ (■), which can be correlated with JCPDS files numbers 77-1971, 21-1272 and 21-949, respectively. Unreacted PbO and TiO_2 phases are detected from the original mixture up to 550 °C, whereas minor amount of $PbTi_3O_7$ is observed at 450 °C and totally disappeared at higher temperature.

By increasing the calcination temperature from 450 to 800 °C, the yield of the tetragonal PT phase increase significantly until at 600 °C, a single phase of $PbTiO_3$ is formed. This study also shows that crystalline tetragonal PT is the only detectable phase in the powder, after calcination in the range 600 to 800 °C. It is to be noted that a large

temperature decrease observed at temperature greater than 850 °C in the DTA curve may be attribute to the PbO volatilisation, in consistent with other work.[20,40,141,142]

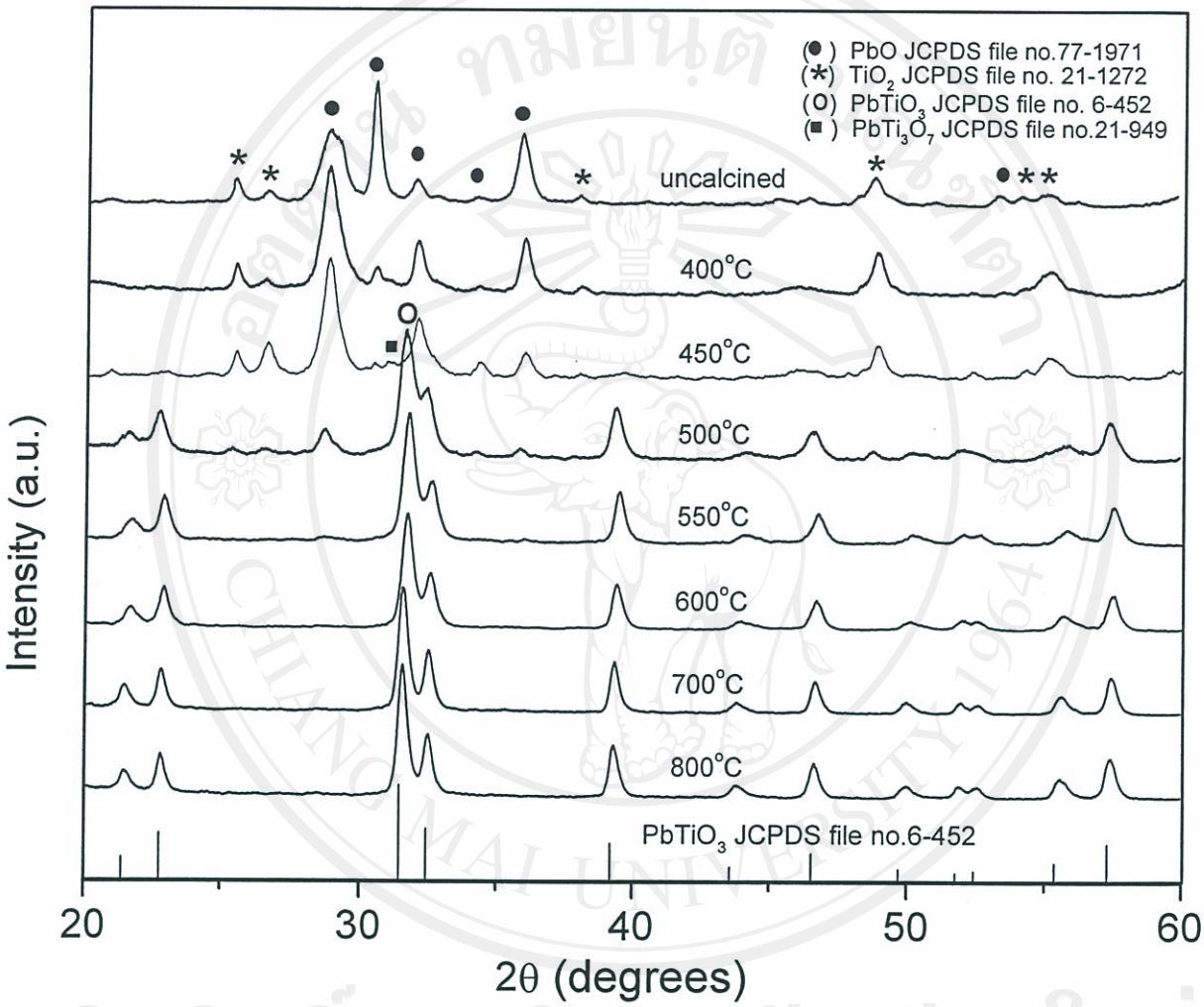

Fig. 4.27 XRD patterns of PT powder calcined at various temperatures for 1 h with heating/cooling rates of 10 °C/min.

Having established the optimum calcination temperature, alternative dwell times ranging from 0.5 to 4 h with constant heating/cooling rates of 10 °C/min were applied at 600 and 550 °C, as shown in Figs. 4.28 and 4.29, respectively. In Fig. 4.28, the single phase of perovskite PT (yield of 100% within the limitations of the XRD technique) was found to be possible only in powders, calcined at 600 °C with soaking time of 1 h or more. The appearance of PbO and $PbTi_3O_7$ phases indicated that full crystallization have not occurred at relatively shorter calcination times. However, in the work reported here, it is to be noted that single–phase of PT powder was also successfully obtained for a calcination temperature of 550 °C with soaking time of 4 h applied (Fig. 4.29). This is probably due to the effectiveness of vibro-milling and a carefully optimised reaction. The observation that the soaking time effect may also play an important role in obtaining a single-phase perovskite product is also consistent with other similar systems.[12-13]

Apart from the calcination temperature and soaking time, the effect of heating/cooling rates on the formation behaviour of PT was also investigated. Five heating/cooling rates (3, 5, 10, 15 and 20 °C/min) were selected for calcination condition of 550 °C/4h (Fig. 4.30) and 600 °C/1h (Fig. 4.31). In this connection, it is shown that the yield of PT phase did not vary significantly with heating/cooling rates, indicating that fast heating/cooling rates can leads to full crystallization of PT phase without time for the formation of pyrochlore phase or lead vaporization. The observation that faster heating/cooling rates are required for lead-based ferroelectrics is also consistent with other investigators.[135,136]

Based on the DTA and XRD data, it may be concluded that, over a wide range of calcination conditions, single phase $PbTiO_3$ cannot be straightforwardly formed via a solid state mixed oxide synthetic route. The experimental work carried out here suggests that the optimal calcination conditions for single phase $PbTiO_3$ is 600 °C for 1 h or 550 °C for 4 h with heating/cooling rates as fast as 20 °C/min which is closed to that of

Pillaiand Ravindran[40] (~ 600 °C for 2h). However, the optimal firing temperatures found here are significantly lower than that reported by Jaffe *et al.*[10] and Shirane *et al.*[44] (> 1000 °C).

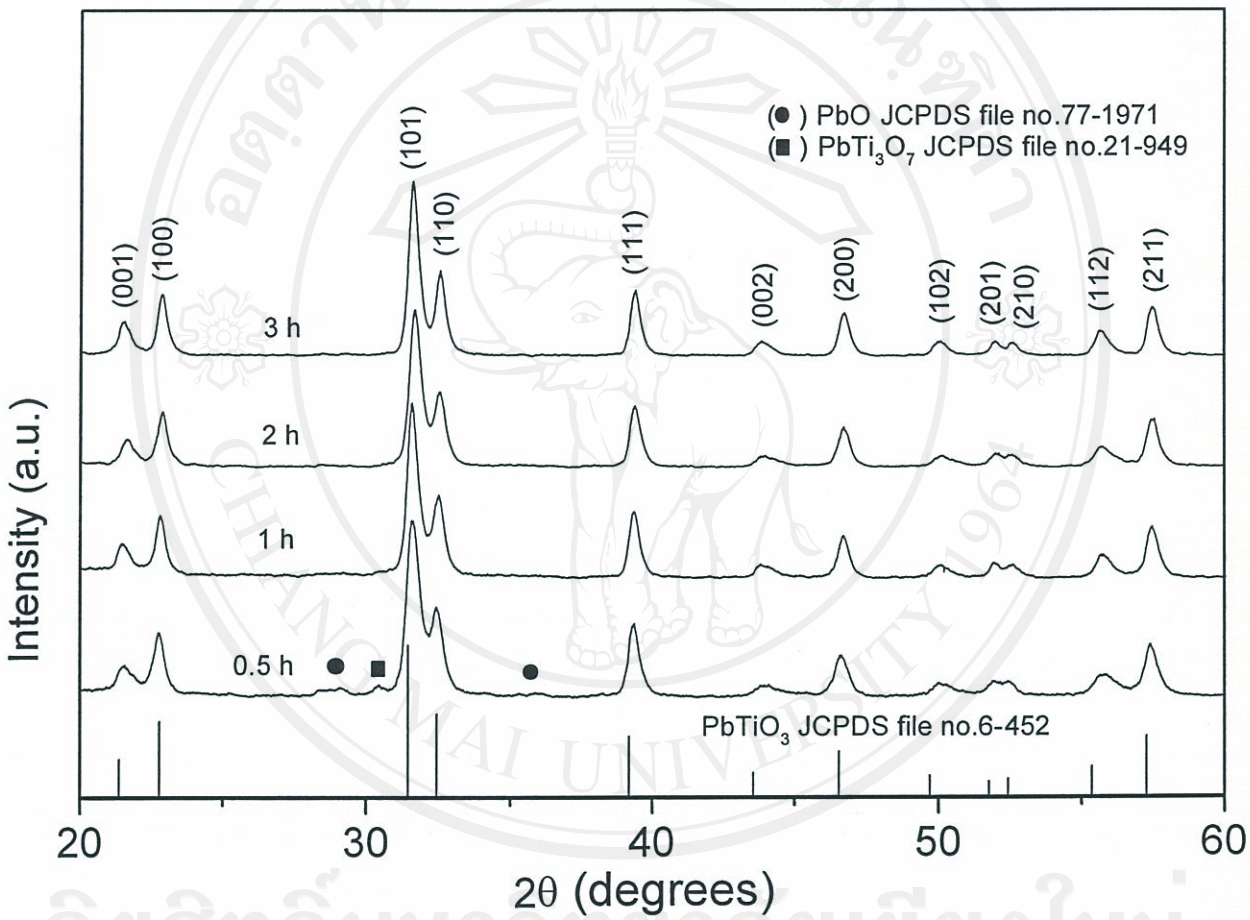

Fig. 4.28 XRD patterns of PT powder calcined at 600 °C with heating/cooling rates of 10 °C/min for various dwell times.

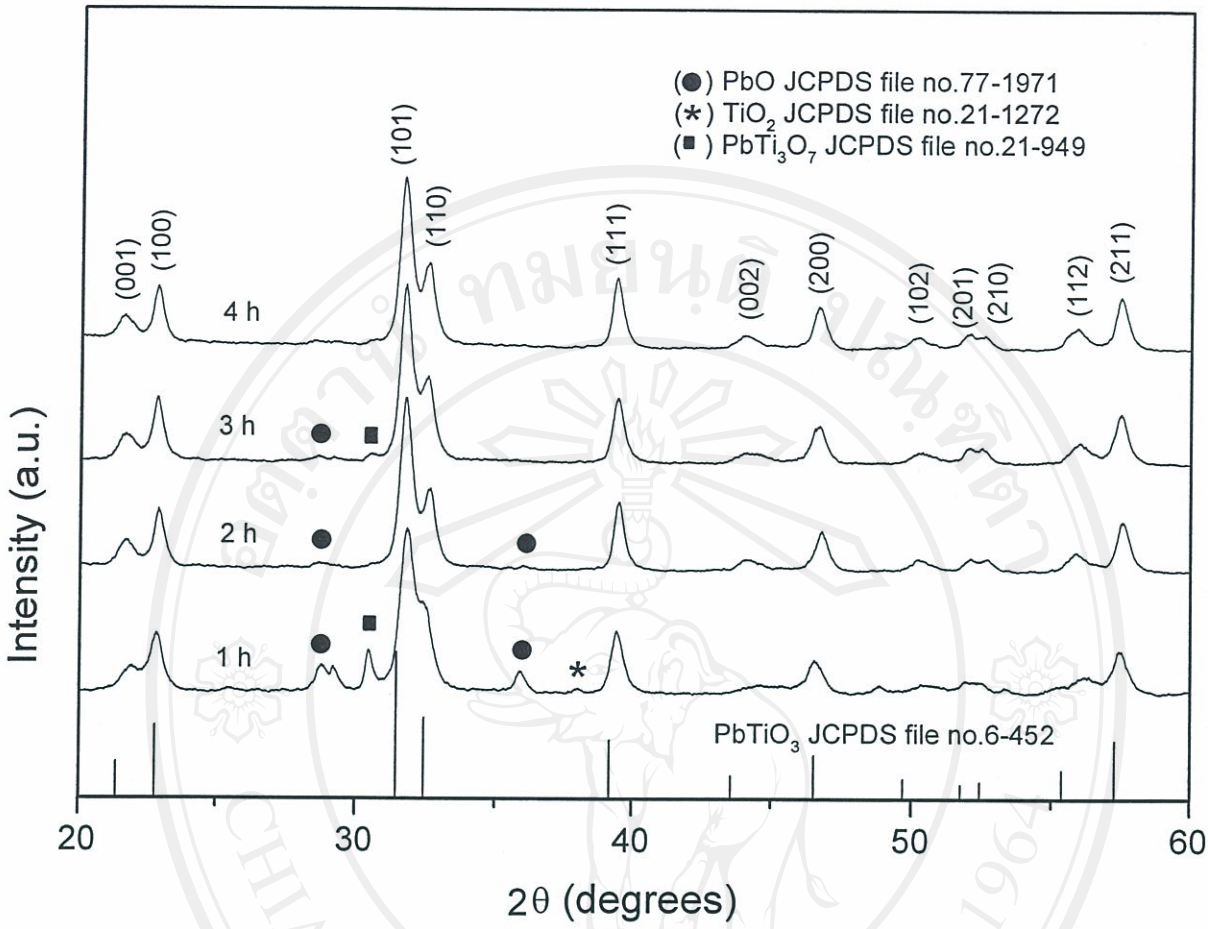

Fig. 4.29 XRD patterns of PT powder calcined at 550 °C with heating/cooling rates of 10 °C/min for various dwell times.

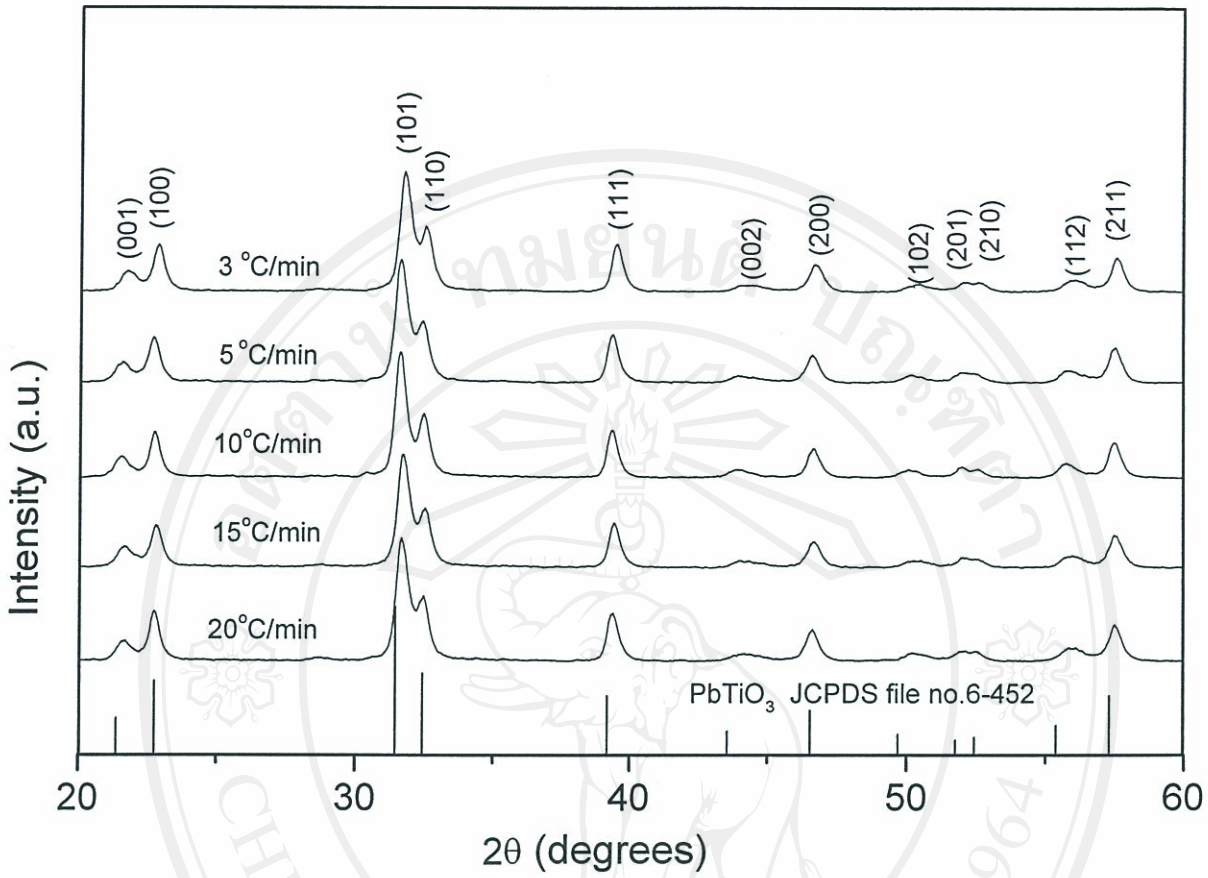

Fig. 4.30 XRD patterns of PT powder calcined at 550 °C for 4 h with various heating/cooling rates.

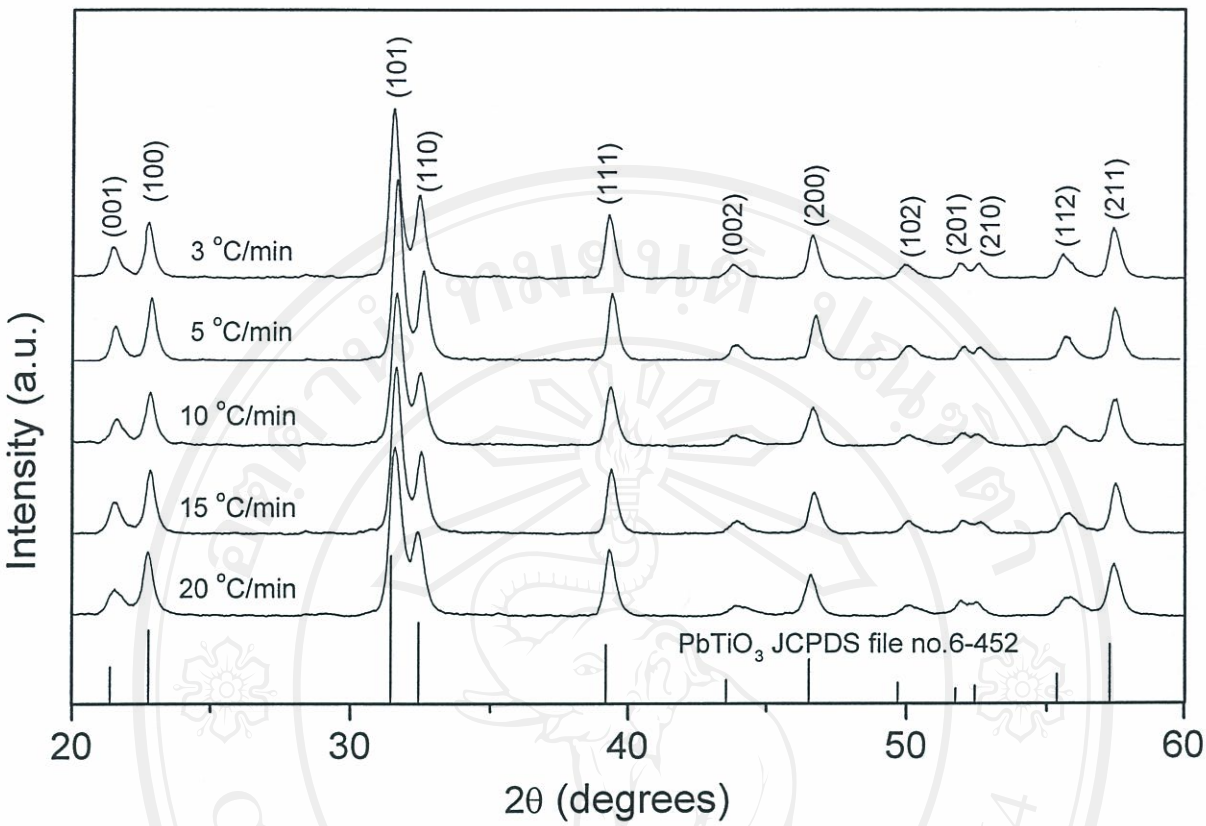

Fig. 4.31 XRD patterns of PT powder calcined at 600 °C for 1 h with various heating/cooling rates.

4.2.1.3 Morphological analysis

Table 4.3 and Fig. 4.32 show particle size and the morphological evolution of all samples as a function of the calcination conditions. In general, the particles are agglomerated and basically irregular in shape, with a substantial variation in particle sizes. The result indicates that degree of agglomeration and grain size tend to increase with calcination temperature and dwell time. However, the smallest particle size (estimated from SEM micrographs to be ~160 nm) and the morphology of the calcined powders are almost the same. It is also of interest to point out that no evidence has been obtained for the existence of the plate-like morphology as that of the hydrothermally derived PT powders.[126]

This work demonstrated that single-phase of lead titanate powders may be produced via this technique by employing a calcination temperature of 550 °C for 4 h or 600 °C for 1 h, with heating/cooling rates of 20 °C/min. The resulting PT powders consist of a variety of agglomerated particles sizes, depending on calcination conditions.

Table 4.3 Phase formation and grain size of PT powders calcined at various conditions.

Calcination temperature (°C)	Dwell time (h)	Heating/cooling rates (°C/min)	Concentration of perovskite phase (%)	Grain size* (μm)
550	4	20	100	0.17-0.32
600	1	20	100	0.16-0.30
600	2	3	100	0.19-0.35
600	2	5	100	0.18-0.37
600	2	10	100	0.20-0.34
600	2	15	100	0.19-0.33
600	2	20	100	0.20-0.36
600	3	20	100	0.21-0.38
700	1	20	100	0.18-0.48
800	1	20	100	0.16-0.55

* These data were taken by estimating from SEM-micrographs

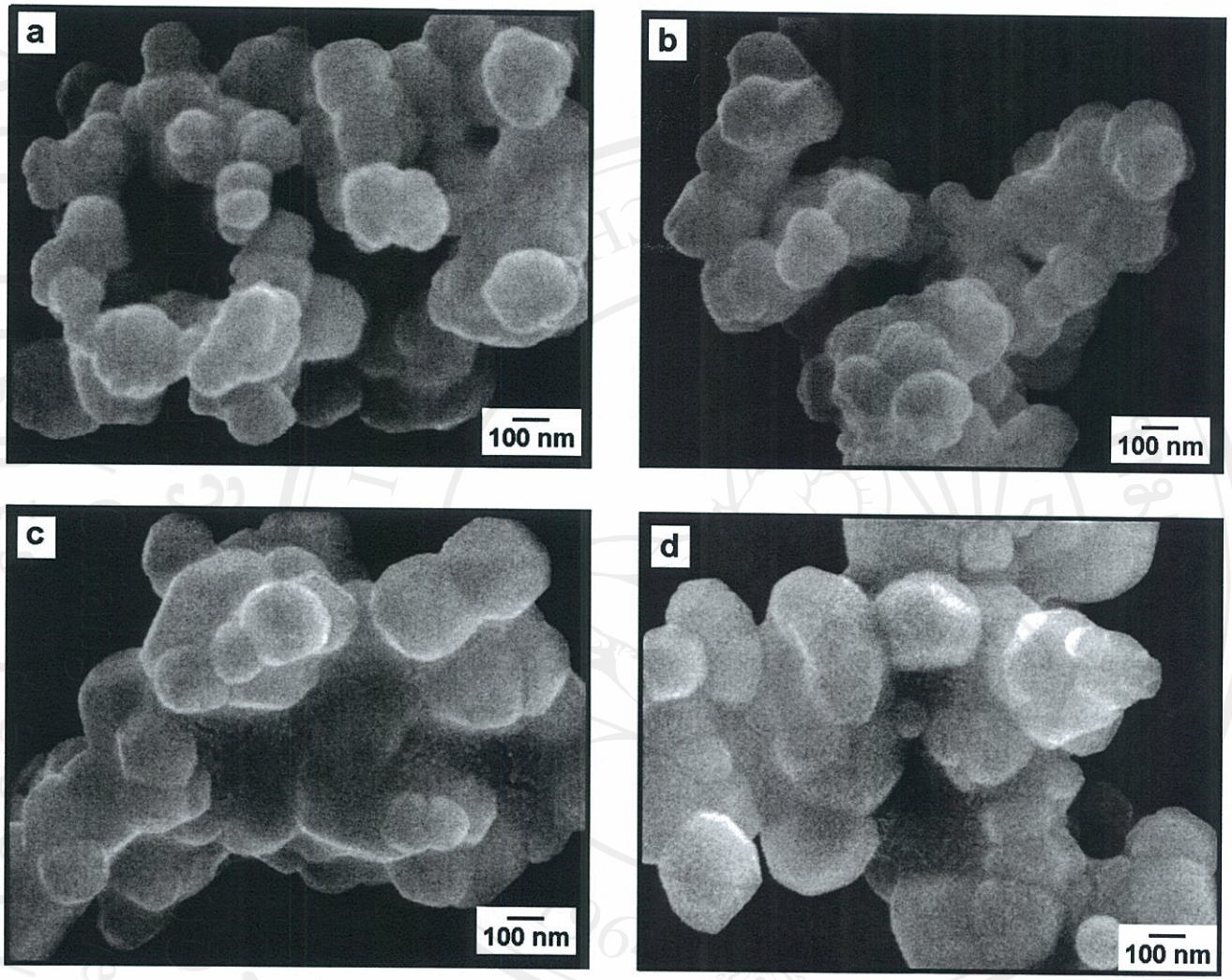

Fig. 4.32 SEM micrographs of the PT powders calcined at (a) 600 °C/1h, (b) 550 °C/4h, (c) 700 °C/1h and (d) 800 °C/1h, with heating/cooling rates of 20 °C/min.

4.2.2 Lead titanate ceramics

4.2.2.1 Phase analysis

Lead titanate (PT) ceramics have been produced by sintering PT powders (section 4.2.1) synthesised from lead oxide (PbO) and titanium oxide (TiO_2). As these PT powders could be prepared in reproducible manner, attention has been focused on relationship between sintering conditions, phase formation, density and microstructural development. The phase formation in the sintered ceramics of sintering temperatures ranging from 1185 to 1230 °C for 2 h, with heating/cooling rate of 3 °C/min are presented via the X-ray diffraction as shown in Fig. 4.33. Table 4.4 presents, percent perovskite phase, relative density, percent shrinkage and percent weight loss.

From Fig. 4.33, it can be seen that the tetragonal PT phase was formed in all PT ceramics, which could be matched with JCPDS file no. 6-452.[125] This is probably due to a combination of the carefully optimized reaction to form single phase precursor powders and the refined sintering procedure. Having established the optimum sintering temperature, alternative dwell times of 1, 2, 3 and 4 h with constant heating/cooling rates of 3 °C/min were applied at 1225 °C (Fig. 4.34). It is seen that the single phase of perovskite PT was found in all dwell times. A dwell time for 2 h was selected for optimal condition in sintering because higher density was obtained here. The constant sintering temperature was used for all samples at 1225 °C for 2 h while heating/cooling rates were varied from 1 °C/min to 10 °C/min. Four heating/cooling rates (1, 3, 5 and 10 °C/min) were selected for sintering condition of 1225 °C for 2 h (Fig. 4.35).

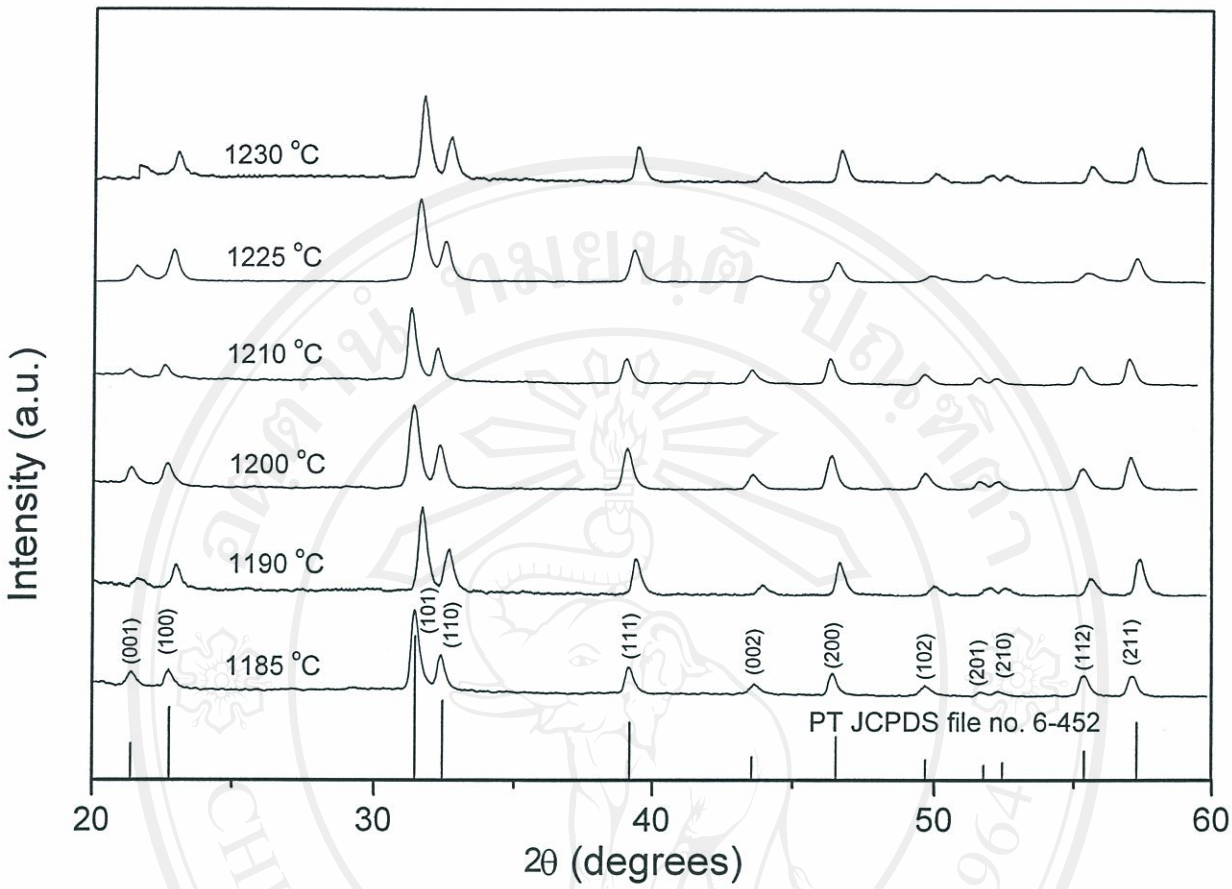

Fig. 4.33 XRD patterns of PT ceramics sintered at various temperatures for 2 h with heating/cooling rates of 3 °C/min.

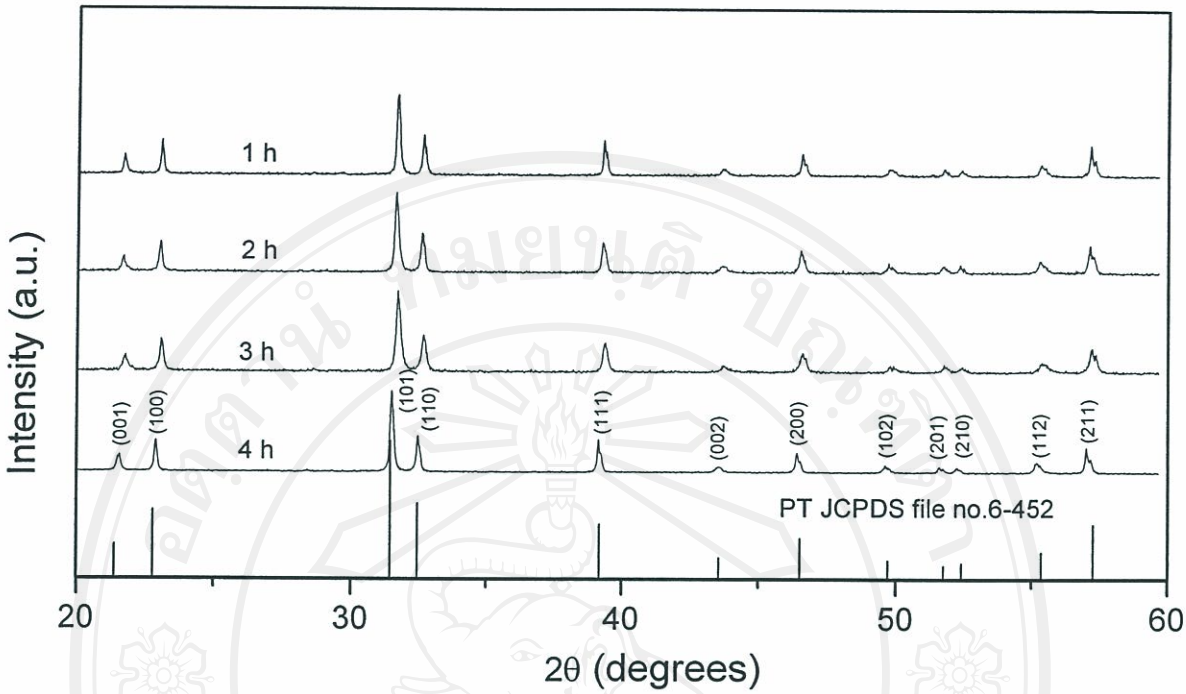

Fig. 4.34 XRD patterns of PT ceramics sintered at 1225 °C °C with heating/cooling rates of 3 °C/min for different dwell times.

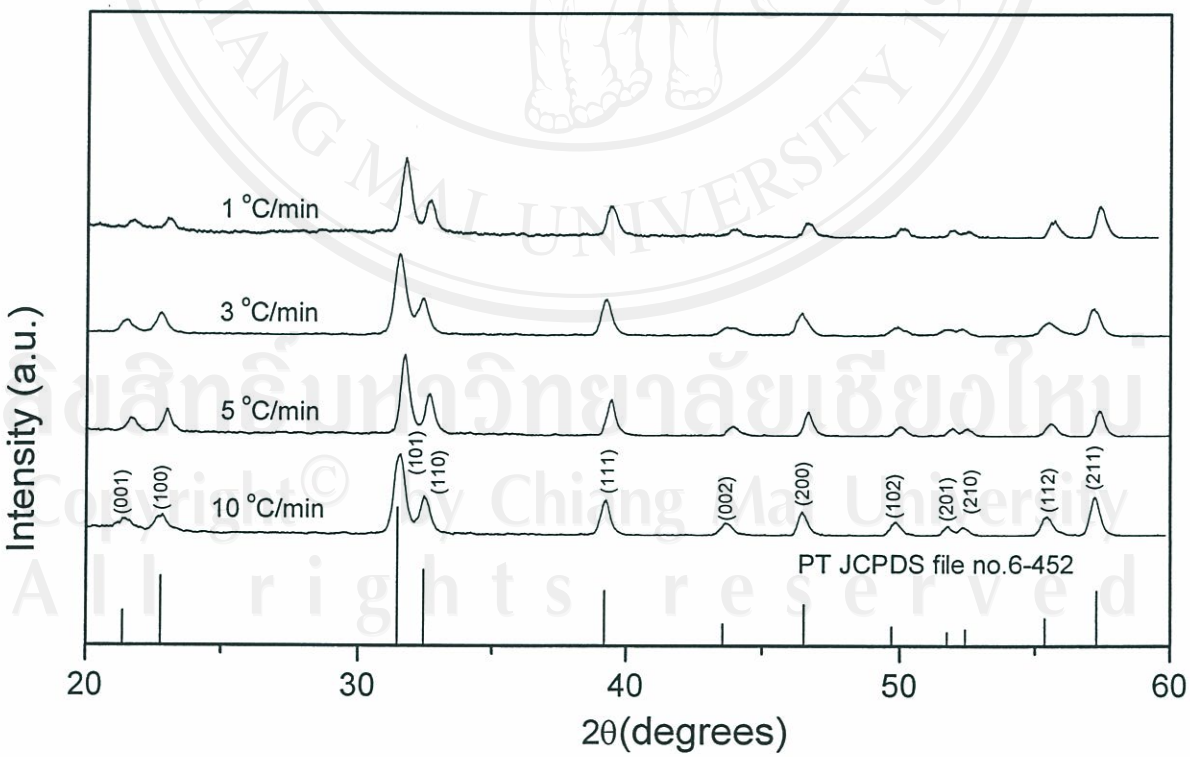

Fig. 4.35 XRD patterns of PT ceramics sintered at 1225 °C for2 h with various heating/cooling rates.

It is seen that only single PT perovskite phases were obtained in all conditions. The degree of tetragonality for each PT ceramics sintered with different heating/cooling rates applied may be calculated from the XRD data as given in Fig. 4.36. In general, it is observed that the tetragonality factor (*c/a* value) tends to increase with the rates, i.e. as the heating/cooling rates increase, the *a*-axis decreases while the *c*-axis increases. Thus, by employing the heating/cooling rates of 1 °C/min where *c/a* is ~ 1.056, serious internal stress commonly found for typical PT ceramics (~ 1 .065)[62], could be significantly reduced and resulting in the formable PT ceramics.

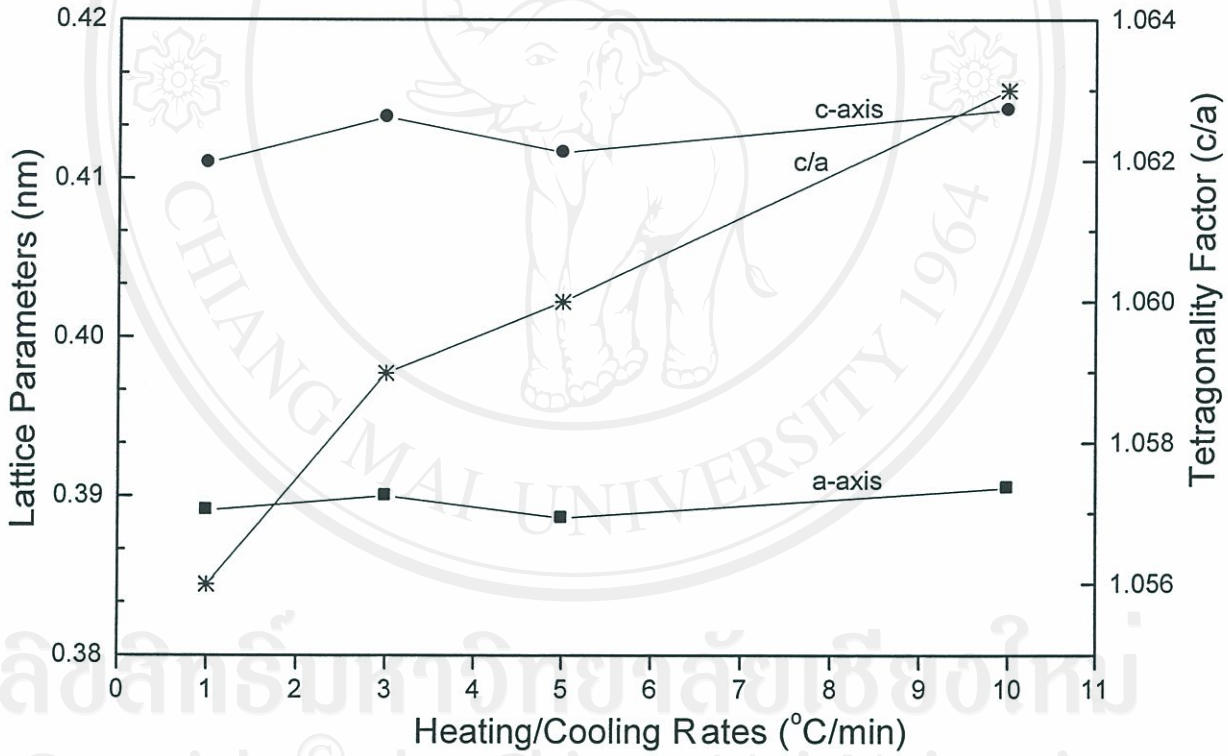

Fig. 4.36 Dependence of lattice parameters and tetragonality factor (*c/a*) in PT ceramics sintered at 1225°C for 2 h with various heating/cooling rates.

Table 4.4 Phase formation and densification of PT ceramics sintered at various sintering temperatures.

Sintering temperature (°C)	Dwell times (h)	Heating/cooling rates (°C/min)	Perovskite (wt%)	Pyrochlore (wt%)	Relative density* (%)	Shrinkage** (%)	Weight Loss*** (%)
1180	2	3	100	0.00	86.70	11.15	9.02
1190	2	3	100	0.00	88.90	11.03	9.15
1200	2	3	100	0.00	89.50	12.18	10.01
1210	2	3	100	0.00	92.70	12.63	10.96
1220	2	3	100	0.00	92.80	13.14	11.56
1225	1	3	100	0.00	91.98	13.98	12.02
1225	2	3	100	0.00	95.40	14.06	12.48
1225	3	3	100	0.00	95.31	14.05	12.51
1225	4	3	100	0.00	91.78	14.04	12.75
1225	2	1	100	0.00	96.80	14.10	12.50
1225	2	5	100	0.00	92.11	14.03	12.49
1225	2	10	100	0.00	92.54	13.99	12.46
1230	2	3	100	0.00	93.50	14.01	13.08

* The estimated precision of the density is ± 1 %
** The estimated precision of shrinkage is ± 0.5 %
*** The estimated precision of weight loss is ± 0.5%

4.2.2.2 Densification analysis

The theoretical density of tetragonal phase of PT ceramics, which was used for the relative density calculations in the sintered samples, was estimated from the lattice parameter data to be ~7.88 g/cm^3(JCPDS file no.6-452).[125] Densities of the sintered samples were determined by using Archimedes principle.

Density, shrinkage and weight loss data of all PT ceramics sintered at various conditions are given in Table 4.4. It is observed that a density of about 88-97 % of the maximum value for PT can be achieved in this study. The maximum density was obtained only in the samples sintered at 1225 °C for 2 h with heating/cooling rates of 1 °C/min. From Fig. 4.37, the observed fall-off in density at higher temperature is probably due to PbO loss impeding the sintering process. The effect of dwell times on density of PT ceramics sintered at 1225 °C with heating/cooling rate of 3 °C/min are also given in Table 4.4. The density was found to increases with dwell time from 1 h to 3 h and then decrease at 4 h (Fig. 4.38). Apart from the sintering temperature and dwell time, the effect of heating/cooling rates on the densification was also investigated. It is seen that density decreases as the rate increases from 1 to 5 °C/min and stables at higher rates (Fig. 4.39). This could be attributed to the increasing of the tetragonality factor at higher rates.

Shrinkage data and weight losses of all samples sintered at various conditions are illustrated in Figs. 4.40-4.42. The change in dimension was gradually increased with sintering temperature at 1190 °C to 1220 °C and nearly constant after 1225 °C. It is seen that the linear shrinkage increased with sintering temperature but did not vary significantly with dwell times. Whereas, in term of the effect of heating/cooling rates it is seen that shrinkage gradually decreased with increasing of heating/cooling rates. In general, the weight loss increases with sintering temperature and dwell times but remains nearly constant with heating/cooling rates.

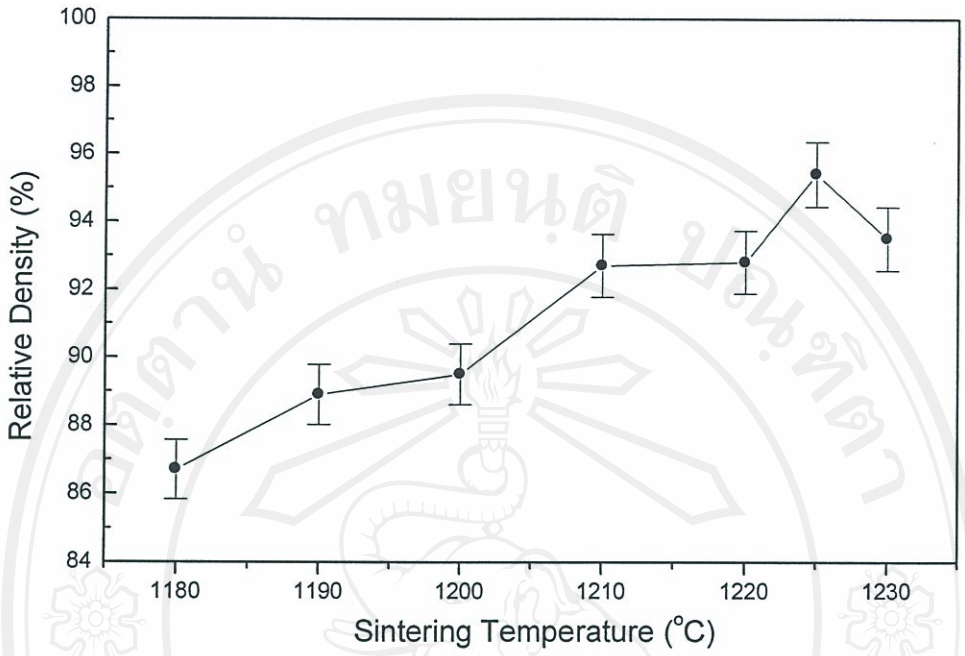

Fig. 4.37 Dependence of relative density in PT ceramics sintered at various sintering temperatures.

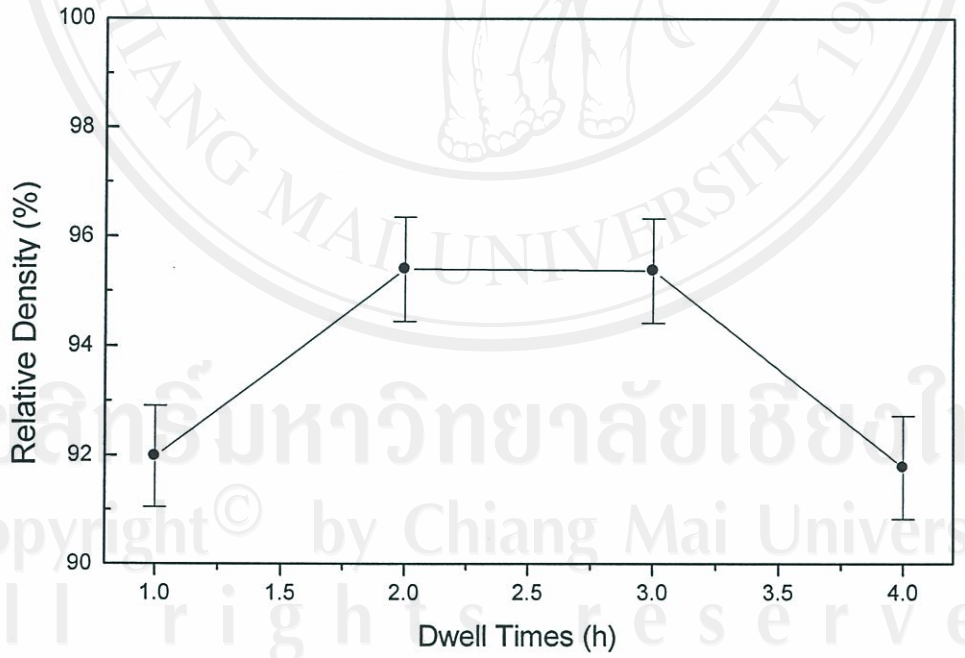

Fig. 4.38 Sintering density as a function of dwell times for PT ceramics sintered at 1225°C with heating/cooling rates of 3 °C/min.

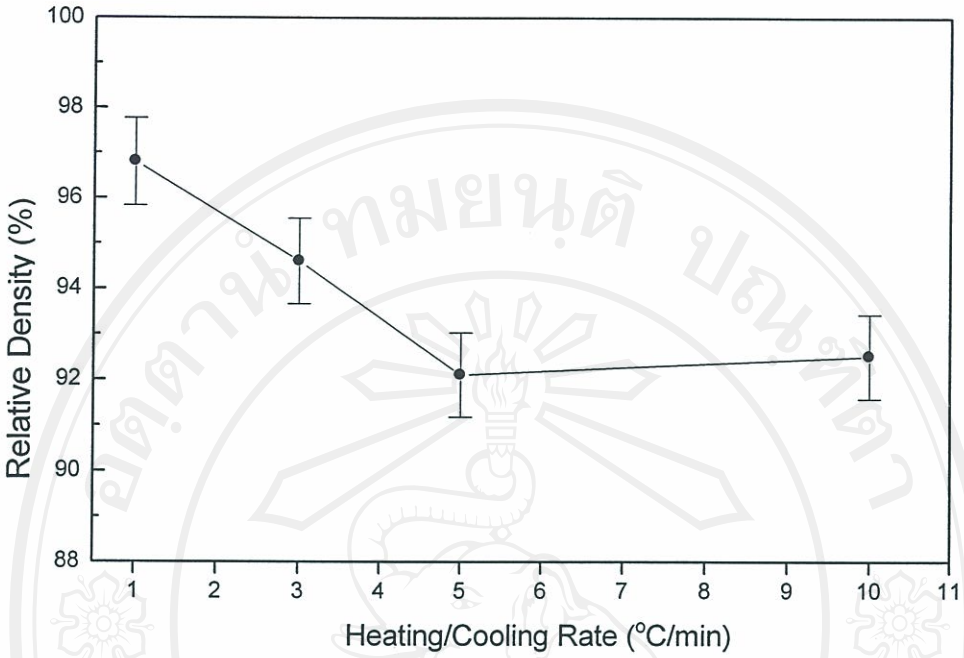

Fig. 4.39 Sintering density as a function of heating/cooling rates for PT ceramics sintered at 1225 °C

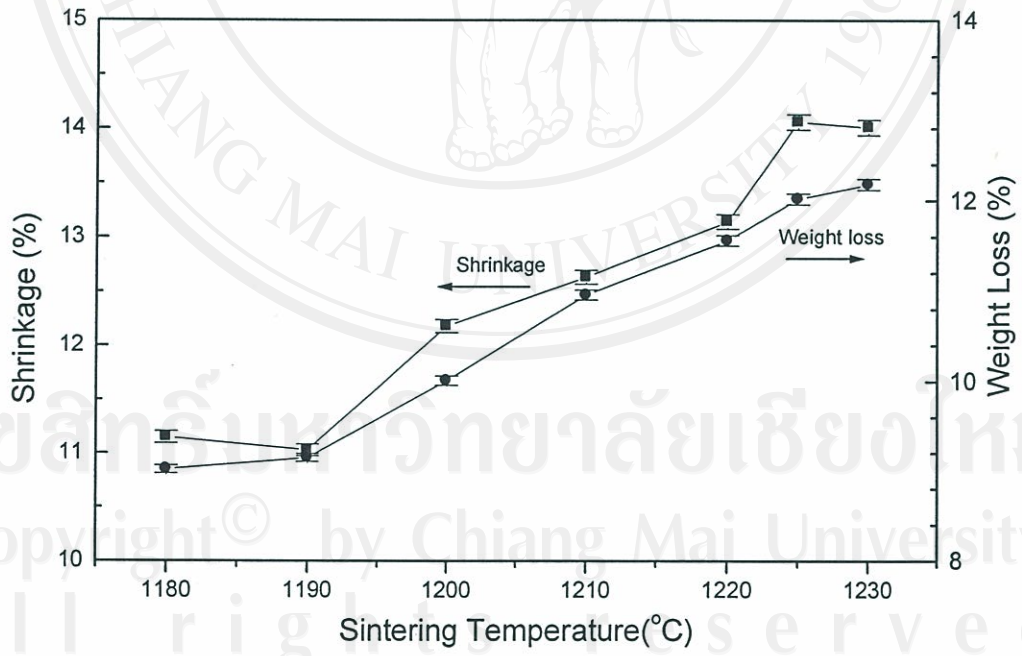

Fig. 4.40 Percentage of shrinkage and weight loss in PT ceramics sintered as a function of sintering temperature.

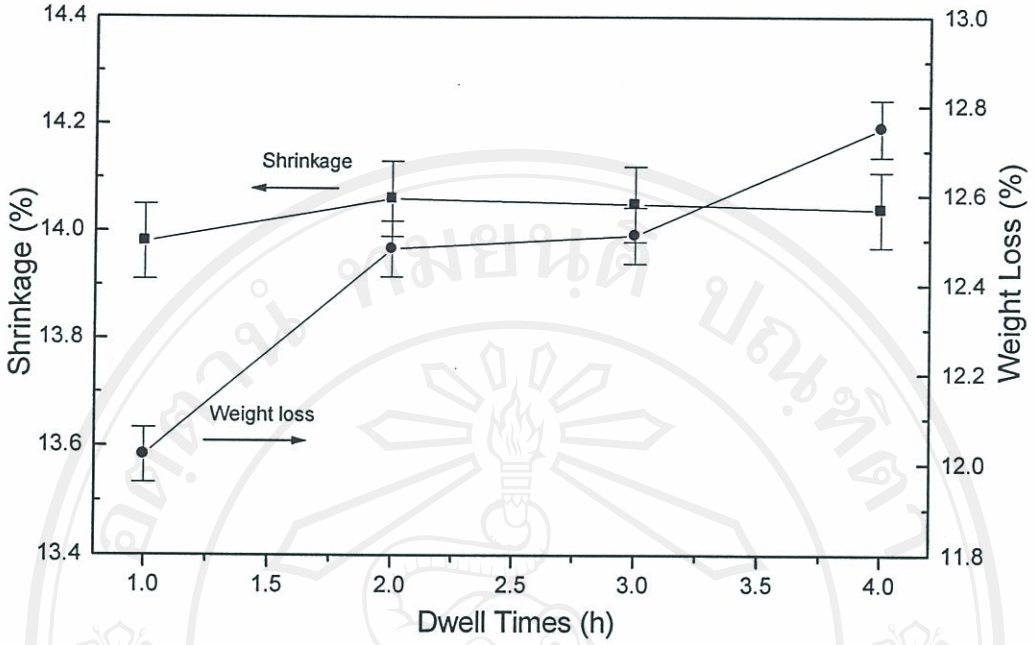

Fig. 4.41 Percentage of shrinkage and weight loss as a function of dwell times for PT ceramics sintered at 1225 °C with heating/cooling rate of 3 °C/min.

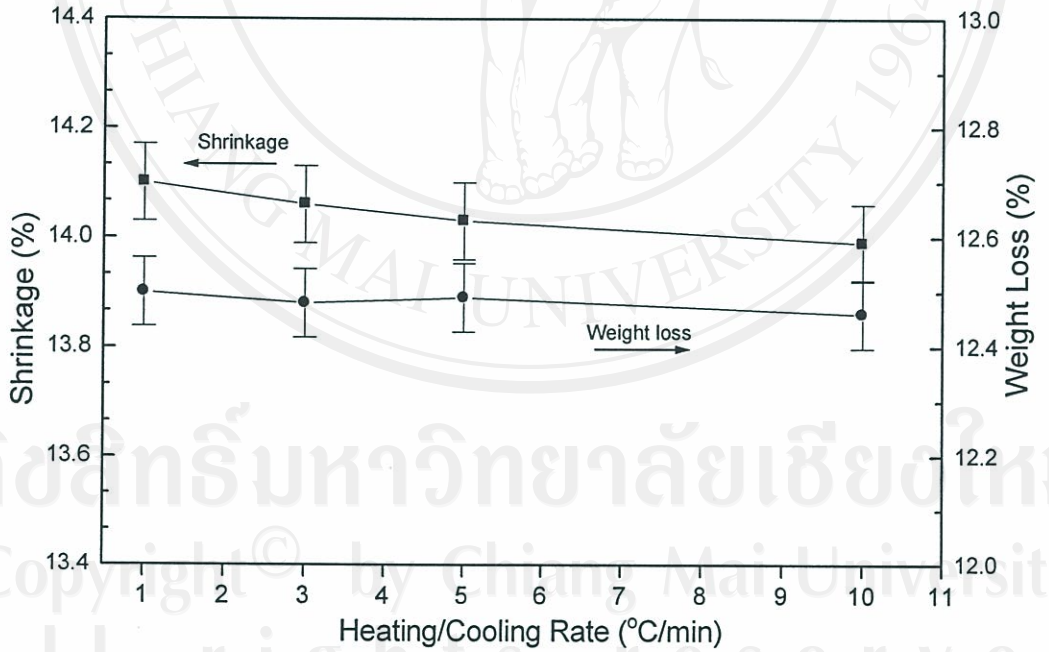

Fig. 4.42 Percentage of shrinkage and weight loss as a function of heating/cooling rates for PT ceramics sintered at 1225 °C.

4.2.2.3 Microstructural analysis

Microstructral development during sintering was investigated by scanning electron microscopy (SEM). Free and fracture surface micrographs of some selected PT ceramics are shown in Figs. 4.43-4.46. Table 4.5 contains the information of grain sizes of the ceramics as function of sintering conditions. The results indicate that average grain size (calculated by linear intercept technique) tends to increase with sintering temperature, dwell times and heating/cooling rates. It should be noted that a pronounced second phase is segregated at the grain boundaries in the samples sintered with heating/ cooling rates of 3, 5 and 10°C/min. This second phase layer is believed to be a PbO-rich composition resulting from a liquid phase formation during the sintering process.[109,127] It is obviously seen that heating/cooling rates are the important parameters for the development of ceramic microstructures. It was also found that the samples with heating/cooling rates of 3, 5 and 10 °C/min eventually burst into pieces because of the internal stresses in the ceramics as can be confirmed by the SEM images showing a loose formation of large grains in Fig. 4.46.

Interestingly, only the samples of 1 °C/min heating/cooling rates remained with the highest relative density and smallest average grain size of about 97% and 0.6 mm, respectively. It may be assumed that, the ceramics consisting of very fine grains suffer less deformation, caused by the high value of *c/a* ratio, than that of the ceramics with significantly large grains. Consequently, the optimum conditions for forming the highly dense PT ceramics in this work are 1225 °C sintering temperature, 2 h dwell time and 1 °C /min heating/cooling rates. In addition, the results from Pillai and Ravindran[40] showed that single phase with average grain size of 3 μm could be formed at 602 °C (875 K) for 16 h. Even though the long period of 16 h dwell time was used, the sintering temperature was relatively low therefore the small grains could be formed in their ceramics. Conversely, high sintering temperature of 1225 °C was used in this work but the ceramics with small average grain size of 0.6 μm were still achieved.

Therefore, the key parameter that controlled the grain growth here would be attributed to the slow heating rate of 1 °C/min. Conclusively, the further investigation should be carried out in order to find out exactly what inhibits grain growth in these PT ceramics while they are subjected to a long heating schedule of slow heating/cooling rates

Table 4.5 Average grain size of PT ceramics sintered at various sintering conditions.

Temperature (°C)	Dwell times (h)	Heating/cooling rates (°C/min)	Average grain sizes * (μm)
1185	2	3	49
1190	2	3	34
1200	2	3	35
1210	2	3	27
1220	2	3	30
1225	1	3	21
1225	2	1	0.6
1225	2	3	23
1225	3	3	34
1225	4	3	75
1225	2	5	26
1225	2	10	31
1230	2	3	52

*Values calculated by linear intercept technique and estimated precision of the grain sized is ± 7%

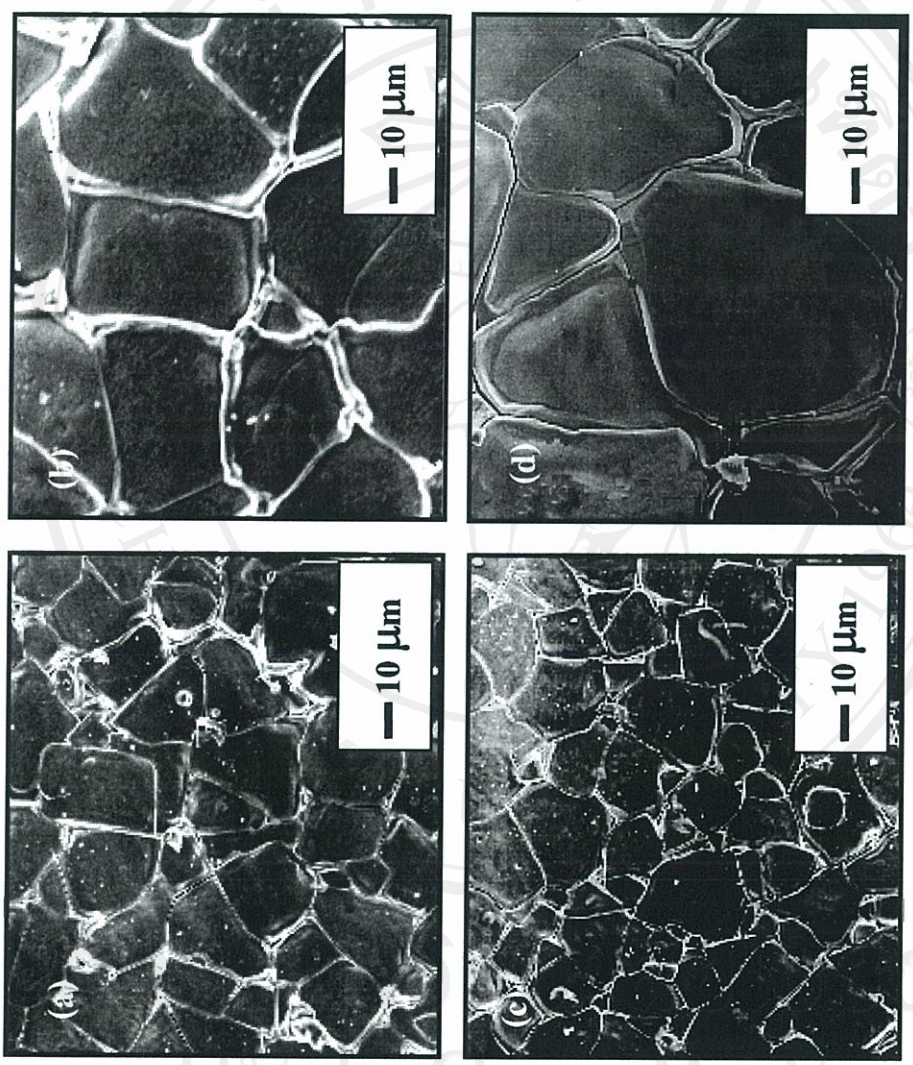

Fig. 4.43 SEM micrographs of the free surfaces of PT ceramics sintered at (a) 1210 °C, (b) 1230 °C, for 2 h and (c) 1225 °C for 1 h, (d) 1225 °C for 4 h, with heating/cooling rates of 3 °C/min.

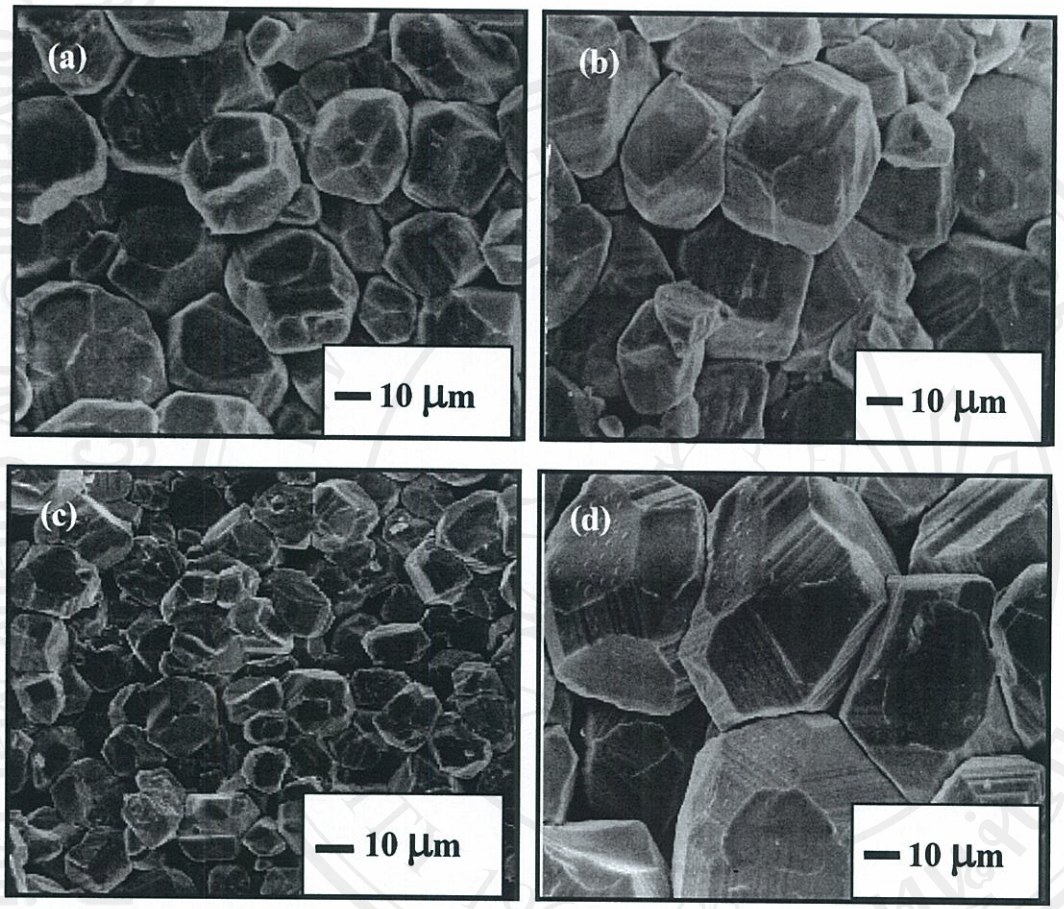

Fig. 4.44 SEM micrographs of the fractured surface of PT ceramics sintered at (a) 1210 °C, (b) 1230 °C, for 2 h and (c) 1225 °C for 1 h, (d) 1225 °C for 4 h, with heating/cooling rates of 3 °C/min.

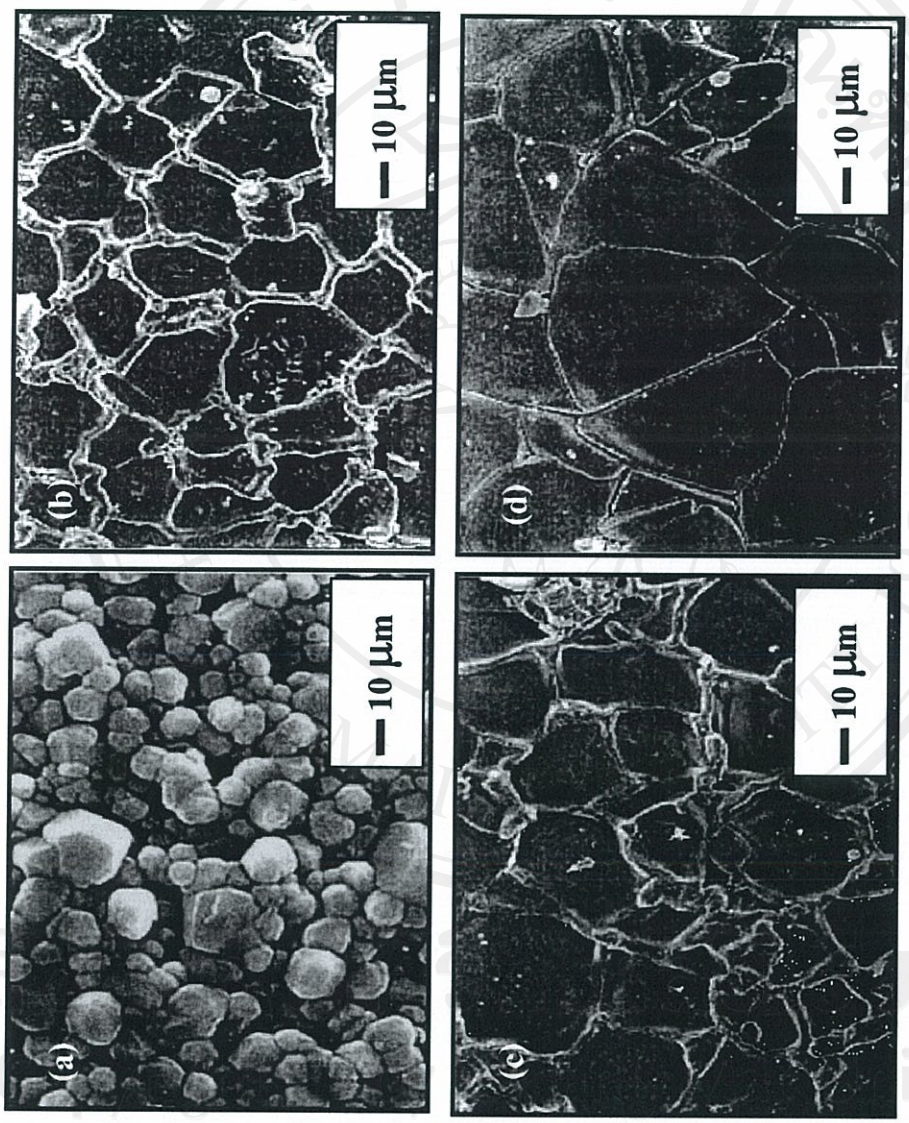

Fig. 4.45 SEM micrographs of the as-fired of PT ceramics sintered at 1225 °C for 2 h, with heating/cooling rates of (a) 1 °C/min, (b) 3 °C/min, (c) 5 °C/min, and (d) 10 °C/min.

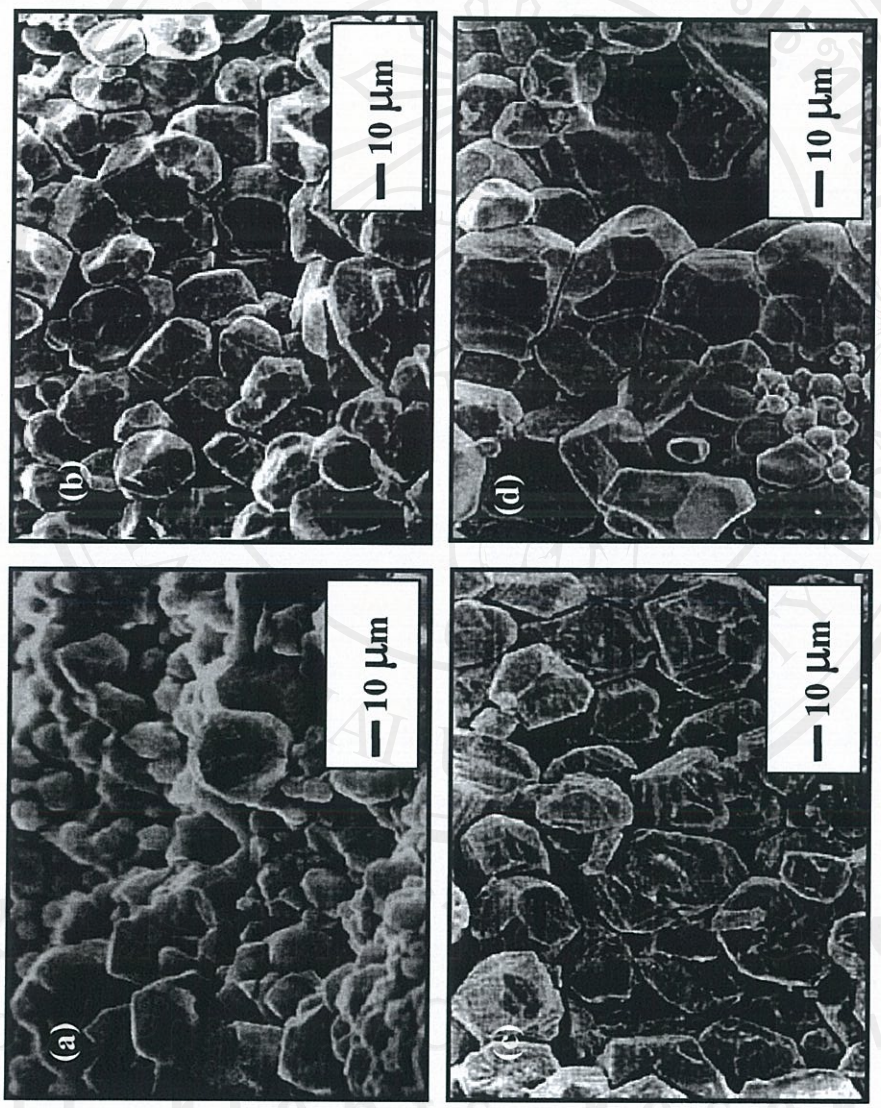

Fig. 4.46 SEM micrographs of the fractured surface of PT ceramics sintered at 1225 °C for 2 h with heating/cooling rates of (a) 1 °C/min, (b) 3 °C/min, (c) 5 °C/min, and (d) 10 °C/min.